Down Syndrome Critical Region 1 Gene, *Rcan1*, Helps Maintain a More Fused Mitochondrial Network

Valentina Parra, Francisco Altamirano, Carolina P. Hernández-Fuentes, Dan Tong, Victoriia Kyrychenko, David Rotter, Zully Pedrozo, Joseph A. Hill, Verónica Eisner, Sergio Lavandero, Jay W. Schneider, Beverly A. Rothermel

***Rationale*:** **The regulator of calcineurin 1 (RCAN1) inhibits CN (calcineurin), a Ca^{2+}-activated protein phosphatase important in cardiac remodeling. In humans, *RCAN1* is located on chromosome 21 in proximity to the Down syndrome critical region. The hearts and brains of *Rcan1 KO* mice are more susceptible to damage from ischemia/reperfusion (I/R); however, the underlying cause is not known.**

***Objective*:** **Mitochondria are key mediators of I/R damage. The goal of these studies was to determine the impact of RCAN1 on mitochondrial dynamics and function.**

***Methods and Results*:** **Using both neonatal and isolated adult cardiomyocytes, we show that, when RCAN1 is depleted, the mitochondrial network is more fragmented because of increased CN-dependent activation of the fission protein, DRP1 (dynamin-1-like). Mitochondria in RCAN1-depleted cardiomyocytes have reduced membrane potential, O_2 consumption, and generation of reactive oxygen species, as well as a reduced capacity for mitochondrial Ca^{2+} uptake. RCAN1-depleted cardiomyocytes were more sensitive to I/R; however, pharmacological inhibition of CN, DRP1, or CAPN (calpains; Ca^{2+}-activated proteases) restored protection, suggesting that in the absence of RCAN1, CAPN-mediated damage after I/R is greater because of a decrease in the capacity of mitochondria to buffer cytoplasmic Ca^{2+}. Increasing RCAN1 levels by adenoviral infection was sufficient to enhance fusion and confer protection from I/R. To examine the impact of more modest, and biologically relevant, increases in RCAN1, we compared the mitochondrial network in induced pluripotent stem cells derived from individuals with Down syndrome to that of isogenic, disomic controls. Mitochondria were more fused, and O_2 consumption was greater in the trisomic induced pluripotent stem cells; however, coupling efficiency and metabolic flexibility were compromised compared with disomic induced pluripotent stem cells. Depletion of RCAN1 from trisomic induced pluripotent stem cells was sufficient to normalize mitochondrial dynamics and function.**

***Conclusions*:** **RCAN1 helps maintain a more interconnected mitochondrial network, and maintaining appropriate RCAN1 levels is important to human health and disease. (*Circ Res*. 2018;122:e20-e33. DOI: 10.1161/CIRCRESAHA.117.311522.)**

Key Words: calcineurin ■ calpain ■ Down syndrome ■ ischemia reperfusion injury ■ mitochondria ■ mitochondrial dynamics

Cardiovascular disease is the leading cause of death worldwide.[1] Restoring blood flow as soon as possible after a myocardial infarction or stroke is essential. However, reperfusion of ischemic tissue (ischemia/reperfusion [I/R]) can itself cause damage through generation of reactive oxygen species (ROS) and Ca^{2+} overload. Mitochondrial function is a critical determinant of the susceptibility of the heart to I/R damage.[2–4] Mitochondria form dynamic networks whose structure is fashioned by the opposing processes of mitochondrial fission and fusion.[5] Increased fusion tends to increase mitochondrial membrane potential ($\Delta\Psi_m$) as well as the $\Delta\Psi_m$-dependent processes of ATP generation, ROS generation, and mitochondrial Ca^{2+} uptake. An array of proteins are involved in the fission/fusion process, including the fission

Editorial, see p 796
Meet the First Author, see p 792

Original received June 15, 2017; revision received January 17, 2018; accepted January 22, 2018. In December 2017, the average time from submission to first decision for all original research papers submitted to *Circulation Research* was 13.60 days.

From the Advanced Center for Chronic Diseases and Center for Molecular Studies of the Cell, Faculty of Chemical and Pharmaceutical Sciences and Faculty of Medicine (V.P., C.P.H.-F., Z.P., S.L.) and Institute of Biomedical Sciences, School of Medicine (Z.P.), University of Chile, Santiago; Department of Internal Medicine/Cardiology (V.P., F.A., D.T., V.K., D.R., Z.P., J.A.H., S.L., J.W.S., B.A.R.) and Department of Molecular Biology (V.K., J.A.H., B.A.R.), University of Texas Southwestern Medical Center, Dallas; and Department of Molecular and Cellular Biology, Faculty of Biological Sciences, Pontificia Universidad Católica de Chile, Santiago (V.E.).

The online-only Data Supplement is available with this article at http://circres.ahajournals.org/lookup/suppl/doi:10.1161/CIRCRESAHA.117.311522/-/DC1.

Correspondence to Beverly A. Rothermel, PhD, Department of Internal Medicine/Cardiology, University of Texas Southwestern Medical Center, 5323 Harry Hines Blvd, Dallas, TX 75390. E-mail beverly.rothermel@utsouthwestern.edu; or Valentina Parra, PhD, Advanced Center for Chronic Diseases (ACCDiS), Faculty of Chemical and Pharmaceutical Sciences, University of Chile, Santiago, Chile. E-mail vparra@ciq.uchile.cl

Novelty and Significance

What Is Known?

- The regulator of calcineurin 1 gene (*RCAN1*), located on human chromosome 21, encodes a protein that inhibits the protein phosphatase calcineurin.
- Excessive activation of calcineurin in the heart contributes to pathological hypertrophy and the progression to failure.
- Calcineurin promotes mitochondrial fission by dephosphorylating the pro-fission protein DRP1 (dynamin-1-like).
- The hearts and brains of mice lacking RCAN1 are more susceptible to damage from ischemia/reperfusion.
- Down syndrome, a condition caused by triplication of chromosome 21, has been associated with altered mitochondrial function and increased oxidative stress.

What New Information Does This Article Contribute?

- The mitochondrial network is more fragmented in cells deficient for RCAN1 because of a calcineurin-dependent increase in DRP1 activation and mitochondrial fission.
- Cardiomyocytes deficient for RCAN1 have decreased mitochondrial membrane potential, O_2 consumption, generation of reactive oxygen species, and capacity for mitochondrial Ca^{2+} uptake.
- This reduces the capacity of mitochondria to buffer cytosolic Ca^{2+}, thereby increasing damage from Ca^{2+}-activated calpain proteases on reperfusion.
- Overexpression of the RCAN1.1 isoform is sufficient to generate a more fused network and increase oxygen consumption.
- Mitochondria in trisomic induced pluripotent stem cells derived from individuals with Down syndrome are larger and more metabolically active than isogenic, disomic controls. Furthermore, siRNA depletion of RCAN1.1 is sufficient to restore the mitochondrial network and function.

Mitochondria carry out critical functions beyond making ATP, such as acting as sites for Ca^{2+} uptake and mediating cell death or survival. Here we show that RCAN1 helps maintain a functional mitochondrial network in cardiomyocytes and other cell types both in vitro and in vivo. Loss of RCAN1 increases mitochondrial fission while decreasing the capacity for Ca^{2+} uptake. This leaves tissues more susceptible to calpain-mediated damage after ischemia/reperfusion, as occurs with heart attack or stroke. Conversely, excess RCAN1 is sufficient to promote fusion and increase mitochondrial metabolism. Although this is beneficial in the heart, we postulate that in the context of Down syndrome, where RCAN1 levels are chronically elevated, enhanced fusion may both increase generation of reactive oxygen species and interfere with the process of mitochondrial repair.

Nonstandard Abbreviations and Acronyms

AMVM	adult mouse ventricular cardiomyocytes
Atp5b	mitochondrial ATPase synthase beta subunit
CAPN	calpain
CN	calcineurin
D21-iPSC	disomic derivative of T21-iPSC
dKD	double knockdown of RCAN1.1 and RCAN1.4
DRP1	dynamin-1-like
DS	Down syndrome
DSCR1	Down syndrome critical region 1
ETC	electron transport chain
Hk2	hexokinase 2
HSPA9	heat shock protein family A (Hsp70) member 9
iPSC	induced pluripotent stem cells
I/R	ischemia/reperfusion
MEF	mouse embryonic fibroblasts
MFN2	mitofusin 2
NRVMs	neonatal rat ventricular myocytes
OPA1	mitochondrial dynamin-like GTPase
Pfkfb2	6-phosphofructo-2-kinase/fructose-2,6-biphosphatase 2
PINK1	PTEN-induced putative kinase 1
RCAN1	regulator of calcineurin 1
RCAN1.1	exon 1 isoform of RCAN1
RCAN1.4	exon 4 isoform of RCAN1
ROS	reactive oxygen species
Slc2a1	solute carrier family 2 member 1
SPTAN1	α-spectrin
T21-iPSC	iPSC derived from individuals with Down syndrome
WT	wild-type
$\Delta\Psi_m$	mitochondrial membrane potential

protein, dynamin-1-like (DNM1L, typically referred to as DRP1). Diverse posttranslational modifications of DRP1 regulate its activity,[6,7] including dephosphorylation by the Ca^{2+}-activated protein phosphatase, CN (calcineurin), that promotes DRP1 translocation to mitochondria, thereby initiating fission.[8] There is a dramatic increase in cytoplasmic Ca^{2+} during ischemia; however, CN remains relatively inactive because of the low pH caused by a buildup of lactic acid.[9] CAPN (calpains) are Ca^{2+}-activated proteases that also play an important role in I/R damage.[10,11] Similar to CN, they remain inactive in the low pH environment of the ischemic heart but are activated rapidly on reperfusion.

Sustained activation of CN is sufficient to drive pathological hypertrophy of the myocardium, with subsequent heart failure and death.[12] CN activity can be modified by members of the RCAN (regulator of calcineurin) family of proteins that inhibit CN activity through a direct protein–protein interaction.[13,14] The regulator of calcineurin 1 (*RCAN1*) gene encodes 2 isoforms and was initially designated as Down syndrome (DS) critical region 1 (*DSCR1*) because of its location on human chromosome 21.[15] Altered mitochondrial function and increased oxidative stress have long been associated with DS.[16] Exon 1 isoform of RCAN1 (RCAN1.1) is abundant in striated muscle and brain where its expression is relatively constant, whereas expression of exon 4 isoform of RCAN1 (*RCAN1.4*) is under the control of CN, thereby acting as a feedback inhibitor of CN activity.[17] Cardiac-specific overexpression of an *RCAN1* transgene protects the heart from a variety of pathological stresses including I/R,[18–20] whereas the brains and hearts of mice lacking RCAN1 are more sensitive to I/R.[21–23]

Here, we investigate the contribution of RCAN1 to the control of mitochondrial dynamics and function using neonatal rat ventricular myocytes (NRVMs), isolated adult mouse ventricular cardiomyocytes (AMVM), mouse embryonic fibroblasts (MEF), and induced pluripotent stem cells (iPSC) derived from individuals

with DS. We show that depletion of RCAN1 increases mitochondrial fission, lowering metabolic function and capacity for Ca^{2+} buffering, thereby increasing CAPN-mediated damage after reperfusion. Conversely, raising RCAN1 levels is sufficient to increase fusion but may compromise coupling efficiency and respiratory reserve.

Methods

Full methods are provided in the Online Data Supplement. All data, methods, and study materials are also available on request by contacting either Dr Parra (vparra@ciq.uchile.cl) or Dr Rothermel (beverly.rothermel@utsouthwestern.edu).

Results

Depletion of RCAN1 Increases Mitochondrial Fragmentation in Cardiomyocytes

Transmission electron micrographs comparing wild-type (WT) and *Rcan1 KO* hearts showed evidence of increased mitochondrial fragmentation in the *KO* (Figure 1A). There was a decrease in the size of individual mitochondria (Figure 1B) and an increase in their number (Figure 1C). Mitochondrial perimeter decreased (Figure 1D), whereas their circularity index increased (Figure 1E).

To test whether RCAN1-dependent changes in the mitochondrial network were cell-autonomous, siRNAs were used to deplete the RCAN1.1 and RCAN1.4 isoforms from cultured NRVMs, either individually or in combination (dKD) (Online Figure I). Forty-eight hours after siRNA transfection, cells were stained with Mitotracker Green (400 nmol/L; Figure 2A) and quantified for both the number and size of individual mitochondria using volume-reconstitution of confocal Z stacks.[24–26] Consistent with the changes observed in the left ventricular wall of *KO* mice, dKD increased mitochondrial number (Figure 2B) and decreased size (Figure 2C). Depleting RCAN1.1 alone resulted in changes comparable to the dKD, whereas the effect of depleting RCAN1.4, although trending in a similar direction, was not significant. Thus, in this experimental context, the RCAN1.1 isoform had the primary impact on mitochondrial morphology. Electron micrographs of the siRNA-depleted NRVMs showed similar changes (Online Figure IIA through IIE).

Fluorescence recovery after photo bleaching was used to compare the functional connectivity of mitochondria. siRNA-transfected NRVMs were labeled with tetramethylrhodamine followed by photo bleaching of selected regions of the mitochondrial network (Figure 2D). Fluorescence recovery after photo bleaching signal was quantified over time. The rate of recovery and the maximal fluorescence recovered were lower in RCAN1.1-depleted NRVMs compared with controls (Figure 2E through 2G), indicative of decreased mitochondrial connectivity or a lower efficiency for mitochondrial membrane potential recovery. There was no apparent change in total mitochondrial mass, as assessed by either Western blot or flow cytometry (Online Figure IIF through IIH).

Depletion of RCAN1 Increases Translocation of DRP1 to Mitochondria

We postulated that loss of CN inhibition in the Rcan1 KO promotes mitochondrial fission by increasing CN activation of DRP1. Consistent with this, there was an increase in DRP1 protein in the mitochondrial fraction of RCAN1.1-depleted and dKD NRVMs compared with control siRNA or RCAN1.4-depleted NRVMs (Figure 2H and 2I). DRP1 phosphorylation at serine 637, the CN substrate site (Ser^{637} in humans and Ser^{656} in rat), was assessed by immunoprecipitating total DRP1 and then probing with a phospho-Ser^{637}-specific antibody. NRVMs depleted for RCAN1.1 alone or as the dKD showed a decrease in Ser^{637} phosphorylation compared with control siRNA and RCAN1.4-depleted cells (Figure 2J and 2K). Taken together, the changes in phosphorylation and subcellular distribution of DRP1 suggest that RCAN1 helps maintain mitochondrial fusion by suppressing CN-mediated activation of DRP1 and points to the RCAN1.1 isoform playing a primary role in this process. Consistent with RCAN1 acting through CN-dependent control of DRP1, pharmacological inhibition of CN using FK506, or inhibition of DRP1 using Mdivi-1, restored a more fused mitochondrial network to RCAN1.1-depleted NRVMs (Online Figure IIIA through IIIF). To verify the impact of RCAN1 depletion on CN activity, we assessed nuclear translocation of endogenous NFAT1, which increased in RCAN1-depleted NRVMs, indicative of

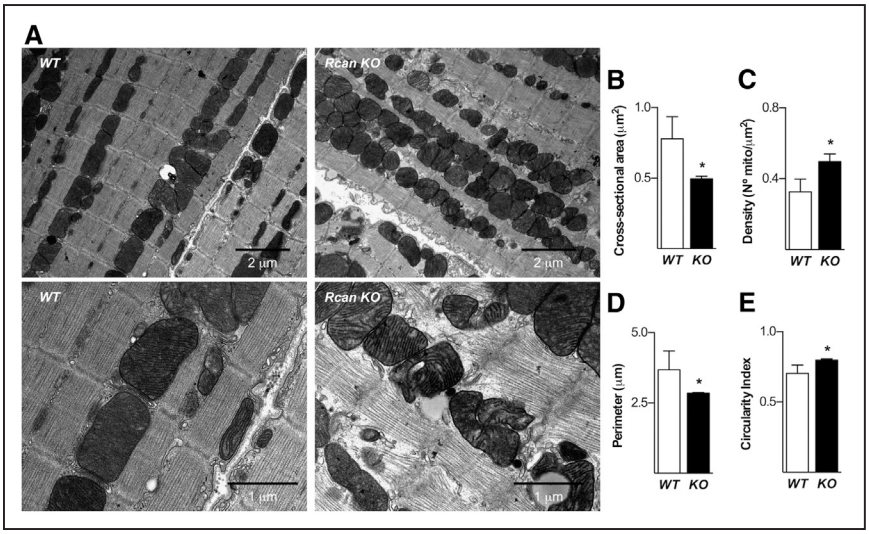

Figure 1. *Rcan1 KO* hearts showed increased mitochondrial fragmentation. **A**, Electron micrographs of the left ventricular wall show disordered and fragmented mitochondria in the knockout (KO) compared to wild-type (WT; scale bar: 1 μm). Mitochondrial were quantified for cross-sectional area (**B**), density (**C**), perimeter (**D**), and circularity index (**E**). One hundred mitochondria were assessed in 3 animals of each genotype (n=3). Mean±SEM; *P<0.05. RCAN1 indicates regulator of calcineurin 1.

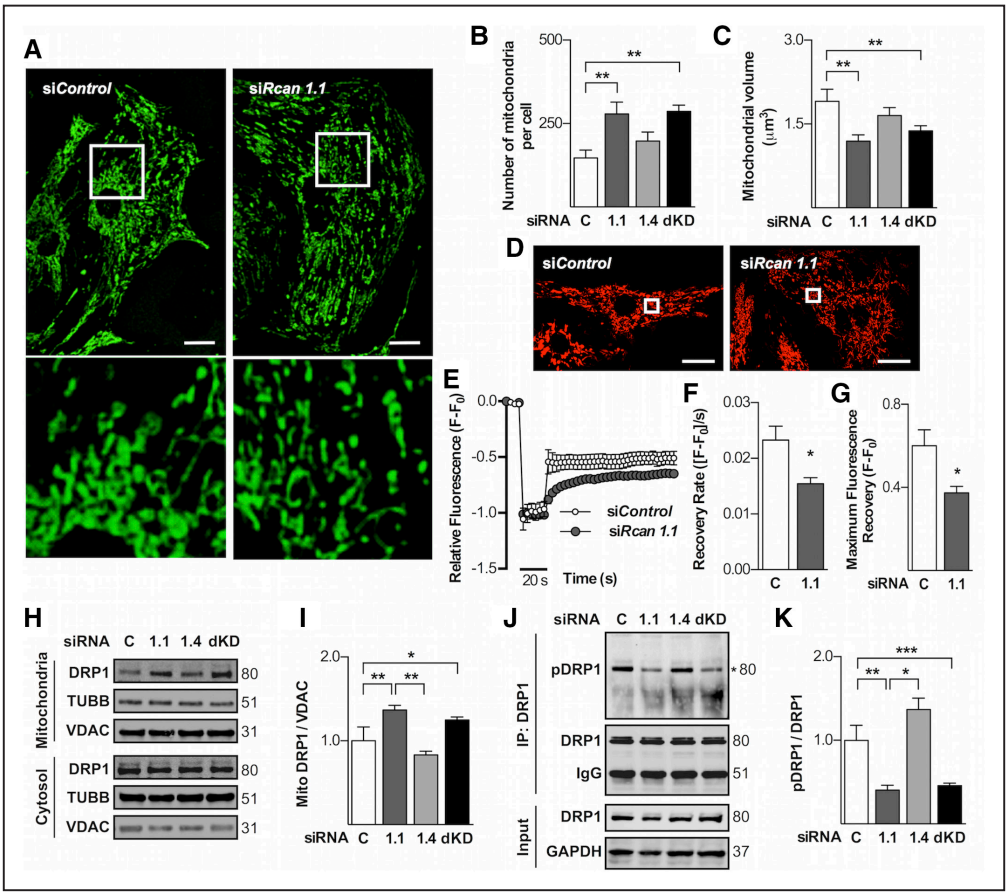

Figure 2. Mitochondrial fragmentation increases in exon 1 isoform of RCAN1 (RCAN1.1)-depleted neonatal rat ventricular myocytes (NRVM). NRVM were transfected with a nonspecific control siRNA or ones targeting *RCAN1.1* and *RCAN1.4*, individually or combined (dKD). **A**, Confocal Z stack reconstructions of si*Control*- and si*RCAN1.1*-depleted NRVMs stained with Mitotracker Green (scale bar: 20 μm) were assessed for (**B**) the number of mitochondria per cell and (**C**) volume of individual mitochondria. Data are from 25 cells examined from 6 separate experiments (n=6). **D**–**K**, Fluorescence recovery after photo bleaching (FRAP) analysis of tetramethylrhodamine (TMRM)-stained NRVM was used to assess connectivity of the mitochondrial network. **D**, Bleaching of TMRM fluorescence was applied in an ≈25-μm² square at randomly chosen regions (scale bar: 10 μm). **E**, Fluorescence recovery was tracked over time and normalized to the signal prior to bleaching then quantified for (**F**) rate of recovery and (**G**) level of recovery. Data are from 15 cells each condition in 5 separate experiments (n=5). **H**, Mitochondria and cytosol were fractionated from siRNA-transfected NRVM and then assessed by Western blot for the proteins indicated. **I**, DRP1 (dynamin-1-like) localized to the mitochondrial fractions in **H** were quantified by densitometry (n=4). **J**, Total DRP1 protein was immunoprecipitated from total cell extracts of siRNA-transfected NRVM and then probed with antibody specific for phospho-Ser[637]. **K**, Signal was normalized to total DRP1 (n=3). Mean±SEM; **P*<0.05, ***P*<0.01, ****P*<0.001. RCAN1 indicates regulator of calcineurin 1.

an increase in CN activity (Online Figure IIIG and IIIH). Immunocytochemistry likewise showed increased colocalization of DRP1 with mitochondria (Online Figure III-I) along with increased fission (Online Figure IIIJ and IIIK).

Mitochondrial Function Is Reduced in Cardiomyocytes Depleted of RCAN1.1

Disruption of the mitochondrial network is often associated with a decrease in mitochondrial function.[5,27,28] Indeed, intracellular ATP (Figure 3A) and $\Delta\Psi_m$ (Figure 3B) were significantly reduced in the RCAN1.1-depleted and dKD NRVMs. $\Delta\Psi_m$ is generated by proton pumping through the mitochondrial electron transport chain (ETC) at complexes (I, III, and IV) and then dissipated through complex V to generate ATP (OXPHOS coupling; Figure 3C). Dissipation of the proton gradient can also occur through other mechanisms, some of which consume ATP. Thus, reductions in $\Delta\Psi_m$ and ATP levels per se do not necessarily indicate a reduction in mitochondrial activity. The rate of O_2 consumption was used to assess electron flow through the ETC and fidelity of OXPHOS coupling. Baseline O_2 consumption was reduced in RCAN1.1-depleted and dKD NRVMs compared with control (Figure 3D). O_2 consumption was lower in RCAN1.1-depleted cells compared with controls, even after the addition of the uncoupler, carbonyl cyanide *m*-chlorophenylhydrazone, indicating a decrease in maximal ETC capacity (Figure 3E). There was no difference between control and RCAN1.1-depleted cells treated with the complex V inhibitor, oligomycin, demonstrating that loss of RCAN1.1 did not alter OXPHOS coupling. Consequently, oligomycin increased $\Delta\Psi_m$ in both control and RCAN1.1-depleted cells (Online Figure IVA). ROS production was also lower in the RCAN1.1-depleted and dKD cells compared with control (Figure 3F and 3G), consistent with a reduction in both their ETC capacity and $\Delta\Psi_m$. It is important to note that mitochondria depleted for RCAN1.1 had the same rate of uncoupled proton leak as control cells, despite a lower

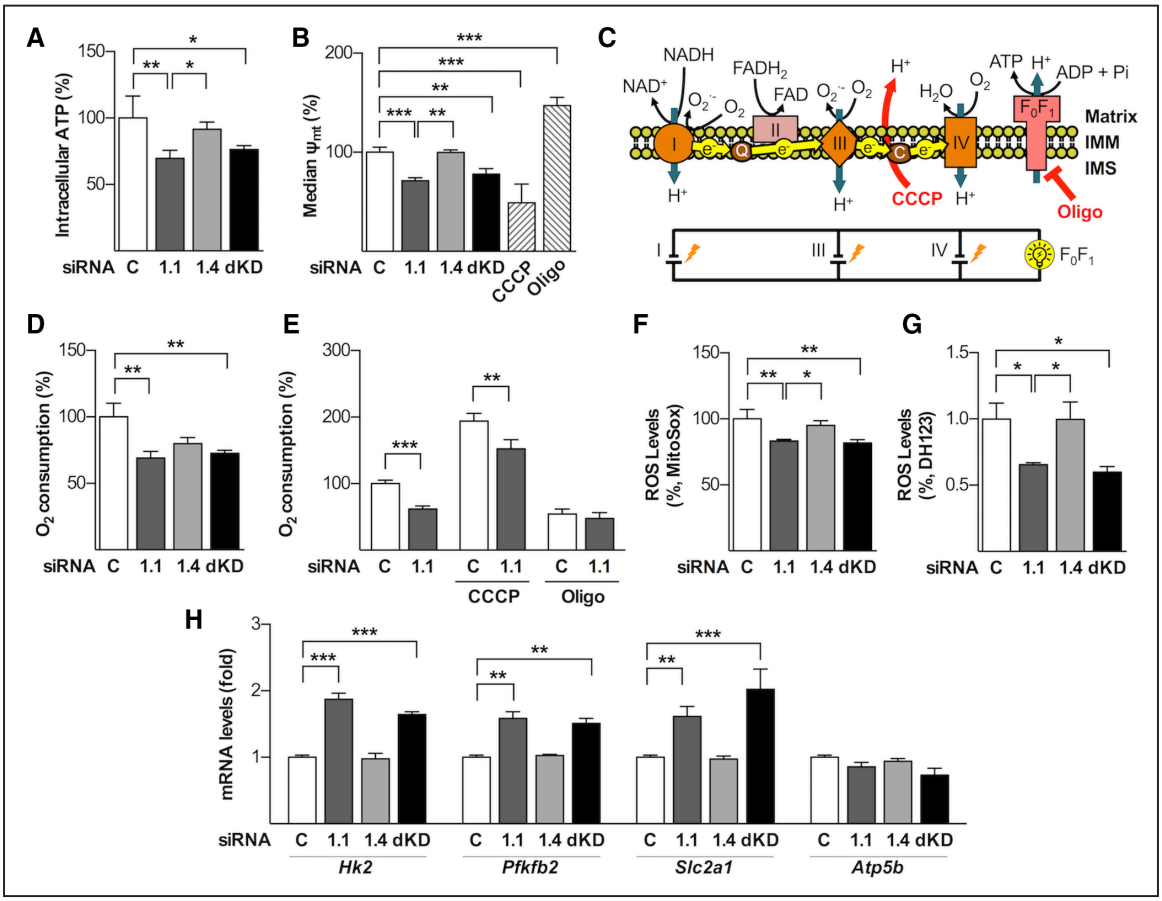

Figure 3. Mitochondrial function is decreased in exon 1 isoform of RCAN1 (RCAN1.1)-depleted neonatal rat ventricular myocytes (NRVM). Cells were transfected with siRNAs as indicated and analyzed 48 h later. **A**, Total cellular ATP levels were measured by luciferase (n=7). **B**, Transfected NRVM were loaded with tetramethylrhodamine (TMRM) and analyzed by flow cytometry to assess $\Delta\psi_m$. The complex V inhibitor, Oligomycin (Oligo, 10 μmol/L), and the mitochondrial uncoupler carbonyl cyanide *m*-chlorophenylhydrazone (CCCP; 50 μmol/L) were used as positive and negative controls, respectively (n=5). **C**, Schematic draws an analogy between mitochondrial electron transport and an electric circuit. Complexes I, III, and IV act in parallel with respect to the proton circuit and in series with respect to the electron flow. The sites of action for Oligo and CCCP are indicated. **D**, O_2 consumption is reduced with RCAN1 depletion (n=6). **E**, Maximal and proton leak–associated O_2 consumption were assessed by adding CCCP (200 nmol/L) or Oligo (50 nmol/L), respectively (n=4). **F**, Total reactive oxygen species (ROS) content was measured by flow cytometry using MitoSox (n=5) or (**G**) DH123 (n=4). **H**, Transcript levels for hexokinase 2 (*Hk2*), 6-phosphofructo-2-kinase/fructose-2,6-biphosphatase 2 (*Pfkfb2*), solute carrier family 2 member 1 (*Slc2a1*), and mitochondrial ATPase synthase beta subunit (*Atp5b*) were quantified by quantitative polymerase chain reaction (qPCR; n=3). Mean±SEM; **P*<0.05, ***P*<0.01, ****P*<0.001. RCAN1 indicates regulator of calcineurin 1.

driving force; ergo, they may be intrinsically leakier. If so, this could further contribute to reducing mitochondrial function and ROS production.

Transcript levels for several genes associated with glycolysis increased, including hexokinase 2 (*Hk2*), 6-phosphofructo-2-kinase/fructose-2,6-biphosphatase 2 (*Pfkfb2*), and solute carrier family 2 member 1 (*Slc2a1,* also known as *Glut1*; Figure 3H), suggesting that the RCAN1.1-depleted and dKD NRVMs may compensate for a reduction in mitochondrial function by increasing reliance on glycolysis. The survival rate of RCAN1.1-depleted NRVMs after a shift to media lacking glucose was reduced compared with control cells (Online Figure IVB). There was no change in transcript levels of the mitochondrial ATPase synthase beta subunit (*Atp5b*), consistent with a reduction in mitochondrial efficiency rather than a change in total mitochondrial mass. Treatment with either FK506 or Mdivi-1 was sufficient to prevent the increase in expression of glycolytic genes in RCAN1-depleted NRVMs (Online Figure IVC through IVH).

Increased Mitochondrial Fragmentation Increases Susceptibility of RCAN1.1-Depleted Cardiomyocytes to I/R

Tissues of the *Rcan1 KO* mice are more susceptible to damage from I/R.[21–23] To examine this in a controlled experimental system, we turned to an in vitro model of simulated cardiac I/R (sI/R). NRVMs depleted of RCAN1 were more sensitive to sI/R (Figure 4A), although sI/R itself did not change protein levels of either RCAN1.1 or RCAN1.4 (Online Figure IV-I and IVJ). Depleting RCAN1.1 had the greatest impact on I/R sensitivity, whereas depletion of RCAN1.4 alone was not significant (Figure 4A). Treatment with either FK506 or Mdivi-1 restored resistance to sI/R (Figure 4B and 4C and Online Figure IVK and IVL), suggesting that endogenous RCAN1 protects from I/R damage by suppressing CN-dependent activation of DRP1.

Abundance of the mitochondrial protein mtHSP70 (HSPA9 [heat shock protein family A (Hsp70) member 9]) was similar in control and RCAN1-depleted NRVM both prior to and after

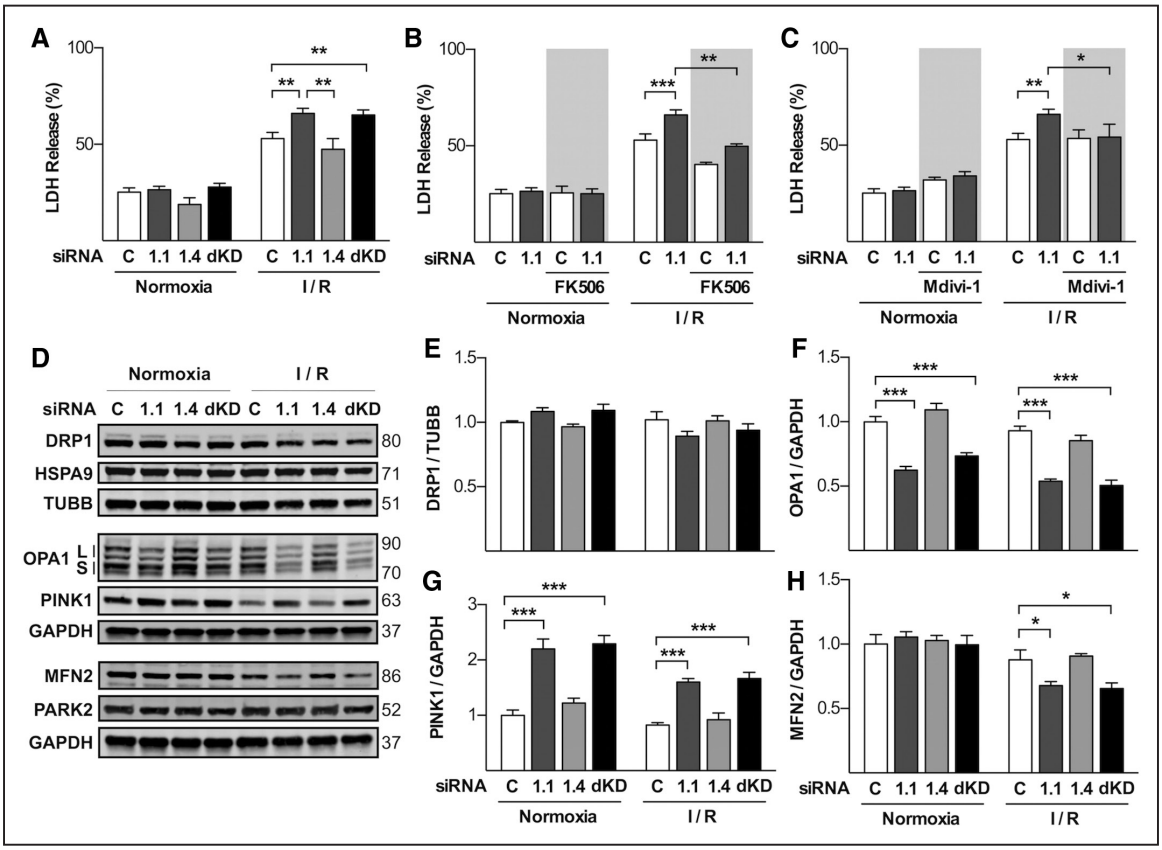

Figure 4. siRCAN1.1-depleted neonatal rat ventricular myocytes (NRVM) are more sensitive to ischemia/reperfusion (I/R) because of calcineurin (CN)-dependent activation of DRP1 (dynamin-1-like). A, Forty-eight hours after transfection, NRVM were subjected to simulated I/R (6 h ischemia and 12 h reperfusion), and LDH (lactate dehydrogenase) release was used to assess death (n=4). **B**, NRVM were treated with either FK506 (20 nmol/L) to inhibit CN or (**C**) Mdivi (12.5 μmol/L) to inhibit DRP1, prior to simulated I/R (n=4). **D–H**, NRVM protein extracts were probed for DRP1, HSPA9 (mtHSP70; heat shock protein family A (Hsp70) member 9), TUBB (β-tubulin), OPA1 (mitochondrial dynamin like GTPase; long and short isoforms), PINK1 (PTEN-induced putative kinase 1), MFN2 (mitofusin 2), PARK2 (Parkinson disease 2), and GAPDH by Western blot and quantified by densitometry (n=4). Mean±SEM; *P<0.05, **P<0.01, ***P<0.001. RCAN1 indicates regulator of calcineurin 1.

sI/R (Figure 4D) suggesting that, at the time points measured, loss of RCAN1 did not alter total mitochondrial mass. Total DRP1 protein levels also remained constant (Figure 4D and 4E). In contrast, levels of all isoforms of the fusion protein, OPA1 (mitochondrial dynamin-like GTPase), were reduced in the RCAN1.1-depleted and dKD NRVMs, both under normoxic conditions and after sI/R (Figure 4D and 4F). There was also an increase in levels of the PINK1 (PTEN-induced putative kinase 1)[29] in the RCAN1.1-depleted and dKD NRVMs, under both normoxic conditions and after I/R (Figure 4D and 4G). Protein levels for the fusion protein, MFN2 (mitofusin 2), were not different under normoxic conditions, but after sI/R, there was a much more pronounced decline in MFN2 in the RCAN1.1-depleted cells compared with controls (Figure 4D and 4H). These changes in OPA1 and MFN2 levels would favor fission and may, therefore, act to further disrupt the mitochondrial network in RCAN1-depleted cells.

The Capacity for Mitochondrial Ca^{2+} Uptake Is Reduced in Cardiomyocytes Depleted of RCAN1.1

Uptake through the mitochondrial Ca^{2+} uniporter is dependent on $\Delta\Psi_m$; thus, a more connected mitochondrial network is a more efficient buffer of cytosolic Ca^{2+}.[30,31] Close proximity of mitochondria to sites of Ca^{2+} release also facilitates mitochondrial Ca^{2+} uptake. In RCAN1.1-depleted NRVMs, there was a general redistribution of mitochondria away from the perinuclear zone (Figure 5A; Online Figure V), a region of close interaction between mitochondria and the endoplasmic reticulum. To assess capacity for mitochondrial Ca^{2+} uptake, NRVMs were loaded with RhodFF and then treated with histamine to evoke Ca^{2+} release from the endoplasmic reticulum. Mitochondrial Ca^{2+} uptake was significantly reduced in RCAN1.1-depleted cells compared with siRNA controls (Figure 5B and 5C). To test the impact on cytosolic Ca^{2+} transients in the setting of calcium-induced calcium release, NRVMs were loaded with Fura2 and then stimulated with 50 mmol/L KCl to depolarize the plasma membrane and trigger calcium-induced calcium release. Cytoplasmic Ca^{2+} levels were similar in RCAN1.1-depleted and control cells at rest. After KCl stimulation, a rapid increase in cytosolic Ca^{2+} was observed in both cell types. However, cytosolic Ca^{2+} returned to baseline levels in the control NRVMs, whereas in the RCAN1.1-depleted cells, cytosolic Ca^{2+} levels remained elevated (Figure 5D and 5E). The increases in cytosolic Ca^{2+} after histamine treatment were also much higher in RCAN1.1-depleted NRVMs compared with those in controls (Online Figure VIA and VIB).

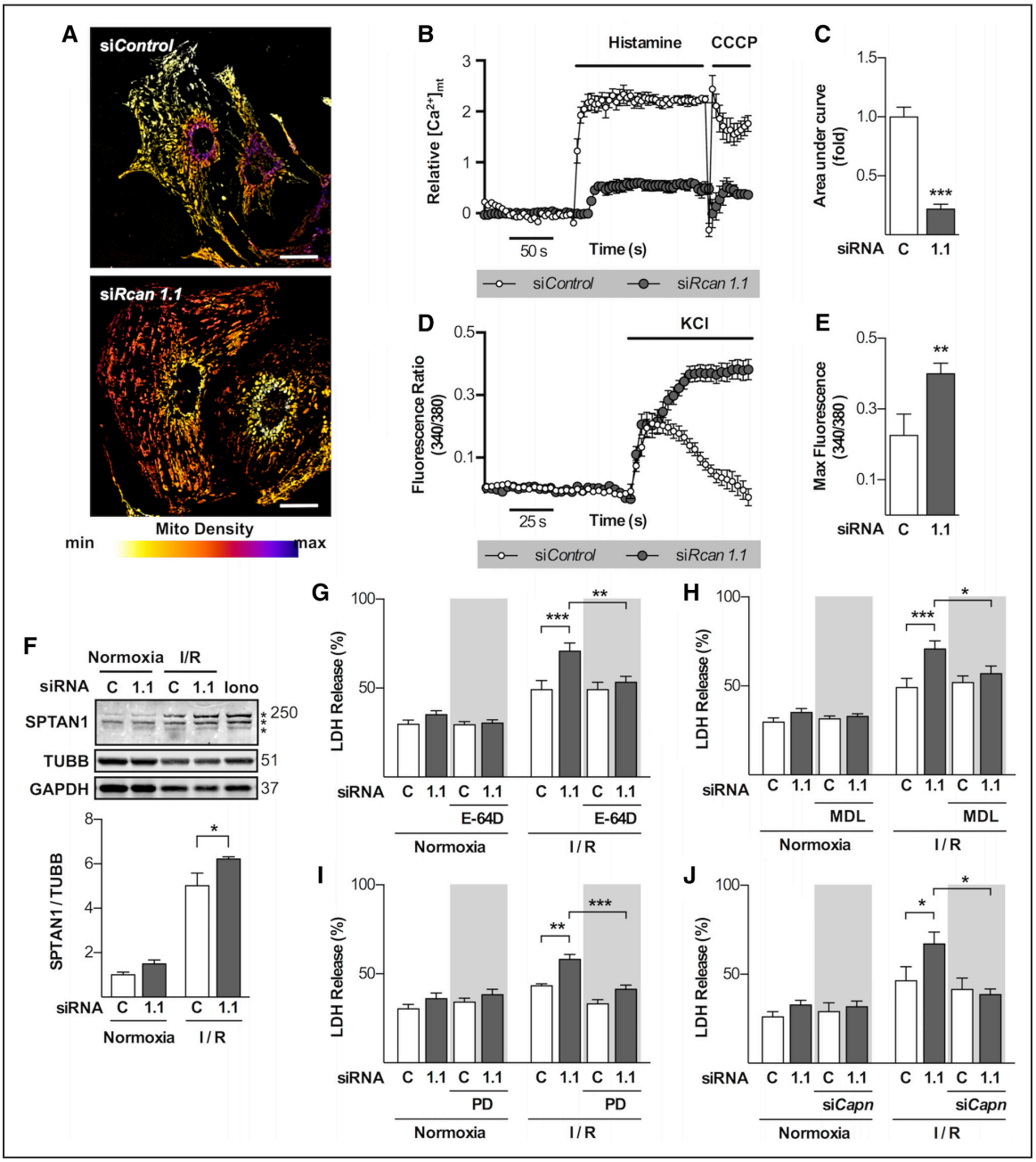

Figure 5. Depletion of exon 1 isoform of RCAN1 (RCAN1.1) reduces mitochondrial Ca^{2+} buffering capacity and increases CAPN (calpain)-mediated damage after ischemia/reperfusion (I/R). A, siRNA-transfected neonatal rat ventricular myocytes (NRVM) stained with Mitotracker Green have been pseudo-colored to indicate the relative density of mitochondrial signal. Yellow indicates lower density, whereas red-violet indicates higher density (scale bar: 20 μm). **B** and **C**, Mitochondria Ca^{2+} uptake was assessed by loading cells with Rhod-FF prior to the addition of histamine (100 μmol/L) to release Ca^{2+} from endoplasmic reticulum (ER) stores (n=4). **D**, Cytosolic Ca^{2+} was assessed by loading cells with Fura2 prior to the addition of KCl 50 mmol/L to trigger Ca^{2+}-induced Ca^{2+} release. **E**, Signal from (**D**) was quantified as the maximal fluorescence ratio reached during the first 150 s. Data are from 50 cells examined in 5 separate experiments. **F**, α-Spectrin (SPTAN1) cleavage products were assessed by Western blot. Ionomycin (Iono) was added as a control for CAPN activation. Quantification in lower panel (n=4). **G–I**, RCAN1-depleted NRVM were treated with the CAPN inhibitors E-64D (10 μmol/L), MDL (10 μmol/L), or PD 150606 (10 μmol/L) prior to simulated cardiac I/R (sI/R; n=5). **J**, A mixture of siRNA's depleting CAPN 1 and 2 (50 nmol/L) also conferred protection to the RCAN1.1-depleted NRVM (n=5). Mean±SEM; *P<0.05, **P<0.01, ***P<0.001. CCCP indicates carbonyl cyanide *m*-chlorophenylhydrazone; RCAN1, regulator of calcineurin 1.

Depletion of RCAN1.1 Increases CAPN-Dependent Cardiomyocyte Damage After I/R

During ischemia, acidification of the cytosol by lactic acid increases cytosolic Ca^{2+} through the combined compensatory actions of the Na^+/H^+ exchanger, the Na^+/K^+-ATPase, and the Na^+/Ca^{2+} exchanger. CAPNs are activated rapidly on reperfusion[32,33] and contribute to the degradation of several structural proteins in cardiomyocytes after I/R, including SPTAN1 (α-spectrin).[34,35] An increase in the levels of SPTAN1 cleavage products after sI/R verified activation of CAPNs in our model (Figure 5F). The accumulation of cleavage products after sI/R was greater in the RCAN1.1-depleted cells than in

control siRNA-treated NRVMs, suggesting increased activation of CAPN. Under normoxic conditions, SPTAN1 cleavage products were not significantly increased in RCAN1-depleted cells compared with controls, suggesting that depletion of RCAN1 does not elevate CAPN activity under homeostatic, resting conditions. Treatment with Mdivi-1 reduced the accumulation of SPTAN1 cleavage products under all conditions (Online Figure VIC and VID). Treatment with any 1 of 3 different CAPN inhibitors (E-64D, MDL, or PD 150606) restored protection from I/R to the RCAN1.1-depleted and dKD cells (Figure 5G through 5I and Online Figure VIE through VIG). E-64D and MDL also inhibit cathepsins.[36] PD 150606 is more specific, inhibiting both CAPN 1 and 2 (μ-CAPN and m-CAPN), which are the primary forms found in heart.[34] Targeted siRNAs were used to knock down both Capn 1 and 2. This conferred significant protection to the RCAN1.1-depleted NRVMs (Figure 5J; Online Figure VIH through VIJ). Preincubation of NRVMs with Ruthenium Red (RuRed), an inhibitor of mitochondrial Ca^{2+} uniporter, increased cell death under normoxia and after I/R in RCAN1.1-depleted cells, whereas, chelating intracellular Ca^{2+} with BAPTA-AM prior sI/R reduced death (Online Figure VIK through VIO). Taken together, these results suggest that NRVMs deficient for RCAN1.1 are more susceptible to damage from I/R because of elevated activation of CAPN after reperfusion and that this may be because of a decrease in mitochondrial Ca^{2+} buffering capacity, the result of enhanced fission.

Increasing RCAN1.1 Levels Is Sufficient to Promote Cardiomyocyte Mitochondrial Fusion and Increase O_2 Consumption

An adenovirus encoding full-length human *RCAN1.1* (*Ad-hRCAN1.1*) was used to test whether increasing RCAN1.1 levels is sufficient to increase mitochondrial fusion (Online Figure VIIA and VIID). Twenty-four hours after infection, *Ad-hRCAN1.1* restored mitochondrial fusion to the RCAN1.1-depleted cells in a dose-dependent fashion (Figure 6A through 6C). In contrast, infection with an adenovirus encoding the RCAN1.4 isoform (*Ad-hRCAN1.4*) was not sufficient to restore the mitochondrial network to RCAN1.1-depleted NRVMs (Online Figure VIIIA through VIIIG). *Ad-hRCAN1.1* also increased fusion in control siRNA cells, demonstrating that increasing RCAN1 levels is sufficient to promote fusion. Consistent with the changes seen in mitochondrial morphology, *Ad-hRCAN1.1* increased O_2 consumption (Figure 6D), ROS generation (Figure 6E), and conferred protection from sI/R (Figure 6F). In contrast, *Ad-hRCAN1.4* did not confer significant protection (Online Figure VIIIH). Although *Ad-hRCAN1.1* infection of control cells increased O_2 consumption, this was at least in part caused by an increase in uncoupling (+oligomycin in Figure 6G) rather than a change in the capacity for maximal electron flow through the ETC (+carbonyl cyanide *m*-chlorophenylhydrazone in Figure 6G).

Loss of RCAN1 In Vivo Decreases Mitochondrial Metabolism and the Capacity for Mitochondrial Ca^{2+} Uptake and Function in Adult Cardiomyocytes

To determine whether our findings in NRVMs translated to the adult myocardium, AMVM were isolated from adult WT and KO mice and evaluated to compare mitochondrial morphology, capacity for Ca^{2+} uptake, and metabolic activity. Despite the compact organization of the mitochondrial network, 3D reconstruction revealed a more fragmented network in KO myocytes compared with WT, with an increase in the total number of mitochondria per cell and a decrease in mitochondrial size (Figure 7A through 7C). Interestingly, separate analysis of interior regions of interest verses peripheral regions of interest suggested that increased fission in the KO localized primarily to mitochondrial populations located in the interior of cardiomyocytes, whereas peripheral populations were not significantly different between KO and WT (Figure 7A, 7D, and 7E). Directly relevant to the increase in I/R sensitivity, the capacity for mitochondrial calcium uptake was significantly reduced in KO AMVM compared with WT (Figure 7F through 7H). The localization of the Ca^{2+} signal was consistent with mitochondrial morphology. Uptake by mitochondrial Ca^{2+} uniporter was validated using the inhibitor RuRed (Online Figure IX). O_2 consumption was measured in permeabilized AMVM. State III respiration was significantly lower in AMVM from the *Rcan1 KO* compared with those from WT using either pyruvate (Figure 7I) or glutamate (Figure 7J) as a substrate. Taken together, these findings indicate that loss of RCAN1 in adult cardiomyocytes replicates many of the key features observed in NRVMs.

Mitochondrial Fusion Is Increased in iPSC Derived From Individuals With Down Syndrome

The preceding studies provide evidence that RCAN1 helps to maintain the mitochondrial network in a more fused configuration and that this affects fundamental metabolic parameters in cardiomyocytes. To determine whether these findings extend to other cell types, we first isolated MEF from the *Rcan1 KO* and compared the mitochondrial network to that of WT MEF. Consistent with the studies in RCAN1-depeleted NRVMs, the mitochondrial network in *Rcan1 KO* MEF showed evidence of increased fission compared with that of WT MEF (Online Figure X); thus, RCAN1's impact on mitochondrial dynamics was not specific to cardiomyocytes. Our studies overexpressing RCAN1.1 in NRVMs also suggest that increasing RCAN1 levels beyond their normal homeostatic controls is not necessarily beneficial and can have detrimental consequences with regard to increased uncoupling and ROS generation (Figure 6).

To examine this in the context of human health and disease, we turned to individuals with DS who are trisomic for chromosome 21. RCAN1 protein levels are elevated in the brain human fetuses with DS,[15,37] and studies have linked RCAN1 with oxidative stress respnses.[38–40] We obtained human trisomy 21 iPSCs (T21-iPSC) and isogenic disomic controls (D21-iPSC) through the PCBC Disease Lines resource (https://progenitorcells.org/).[41] Mitochondrial morphology was assessed and showed a reduction in the number of mitochondria per cell and an increase in the mean volume of individual mitochondria in trisomic T21-iPSC when compared with disomic D21-iPSC, indicative of a more interconnected mitochondrial network (Figure 8A through 8C). The rate of O_2 consumption was also substantially elevated in the T21-iPSC (Figure 8D). O_2 consumption did not further increase after addition of carbonyl cyanide *m*-chlorophenylhydrazone,

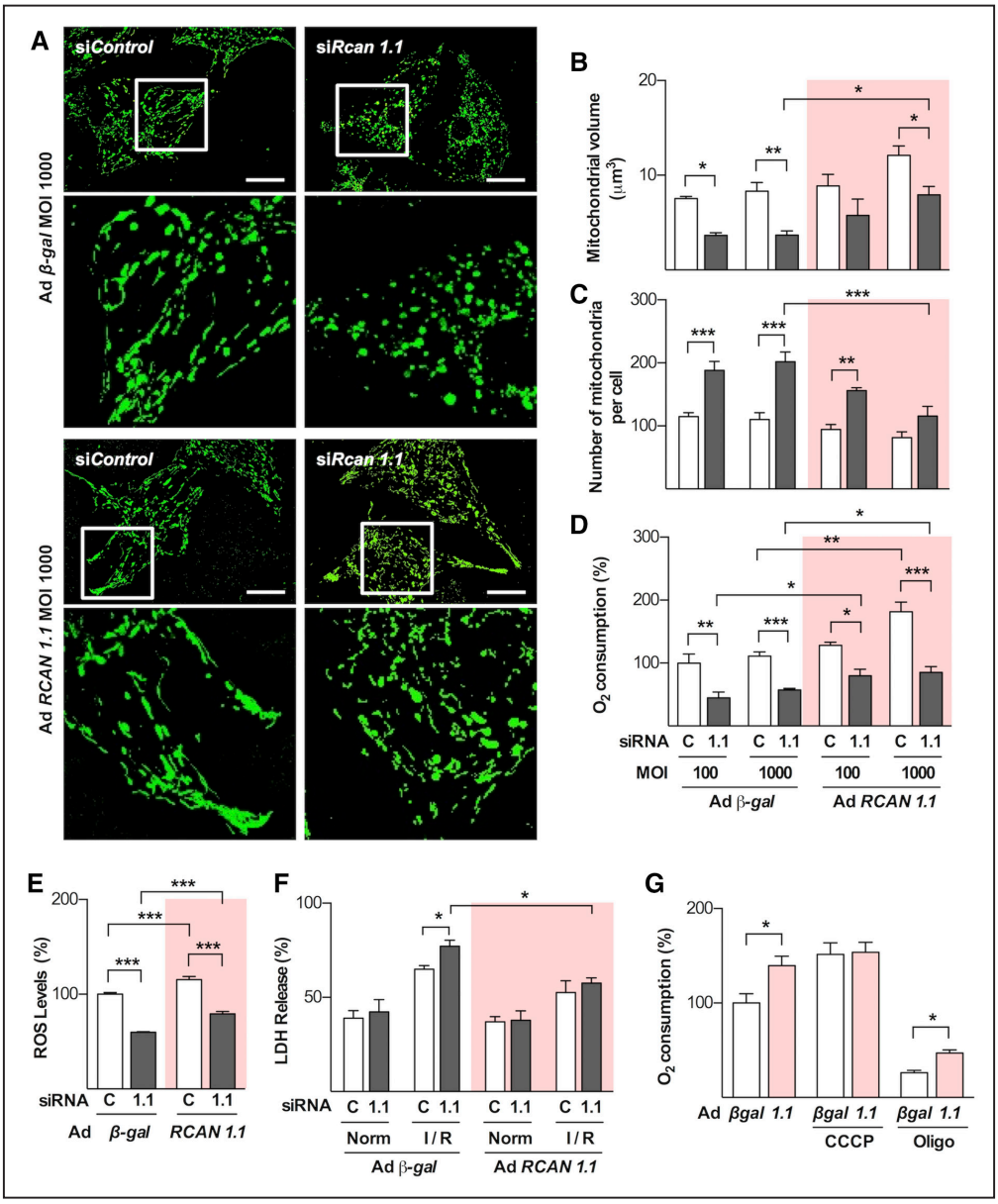

Figure 6. Exogenous expression of human exon 1 isoform of RCAN1 (*RCAN1.1*) restores mitochondrial parameters and protection from ischemia/reperfusion (I/R) to RCAN1.1-depleted neonatal rat ventricular myocytes (NRVM). A, Cells were transfected with indicated siRNAs followed by adenoviral infection to express human *RCAN1.1* (*Ad-RCAN1.1*) or *β-galactosidase* (Ad *β-gal*). Forty-eight hours later, cells were loaded with Mitotracker Green and imaged by confocal (n=4; scale bar: 10 μm) and quantified for (**B**) individual mitochondrial volume and (**C**) the number of mitochondria per cell. **D**, Infection with *Ad-hRCAN1.1* increased O_2 consumption in both si*Control* and si*RCAN1.1*-depleted NRVM (n=4). **E**, Infection with Ad-h*RCAN1.1* increased reactive oxygen species (ROS) production in both si*Control* and si*RCAN1.1*-depleted NRVM (n=4). **F**, Infection with *Ad-hRCAN1.1* restored protection from simulated cardiac I/R (sI/R) to si*RCAN1.1*-depleted NRVM (n=4). **G**, Maximal and proton leak–associated O_2 consumption were assessed by adding carbonyl cyanide *m*-chlorophenylhydrazone (CCCP; 200 nmol/L) or oligomycin (50 nmol/L), respectively, to control cells infected with either *Ad-β-gal* or *Ad-hRCAN1.1* (n=4). Mean±SEM; **P*<0.05, ***P*<0.01, ****P*<0.001. RCAN1 indicates regulator of calcineurin 1.

suggesting that the mitochondria in these cells are already working at maximal capacity. Importantly, there was also an increase in uncoupled proton leak in the T21-iPSC similar to that observed in control NRVMs infected with *Ad-hRCAN1.1* (Figure 6), suggesting that increased dosage of RCAN1 may have detrimental effects on mitochondrial function.

Although chromosome 21 is the smallest of the human somatic chromosomes, it contains over 200 genes along with an array of noncoding RNAs, any one, or combination of, could contribute to this change in mitochondrial morphology and function. To test whether increased dosage of the *RCAN1* gene underlies the changes in mitochondrial form and function, human-specific siRNAs were used to deplete each of the RCAN1 isoforms individually and in combination from the trisomic T21-iPSC. At baseline, transcript levels for *RCAN1.1* were elevated in the T21-iPSC compared with those in the disomic D21-iPSC (Figure 8E). The disomic and trisomic iPSC were transfected with siRNAs targeting *RCAN1.1* and *RCAN1.4* alone or in combination. siRNA targeting *RCAN1.1* was effective at reducing *RCAN1.1* transcript levels in both

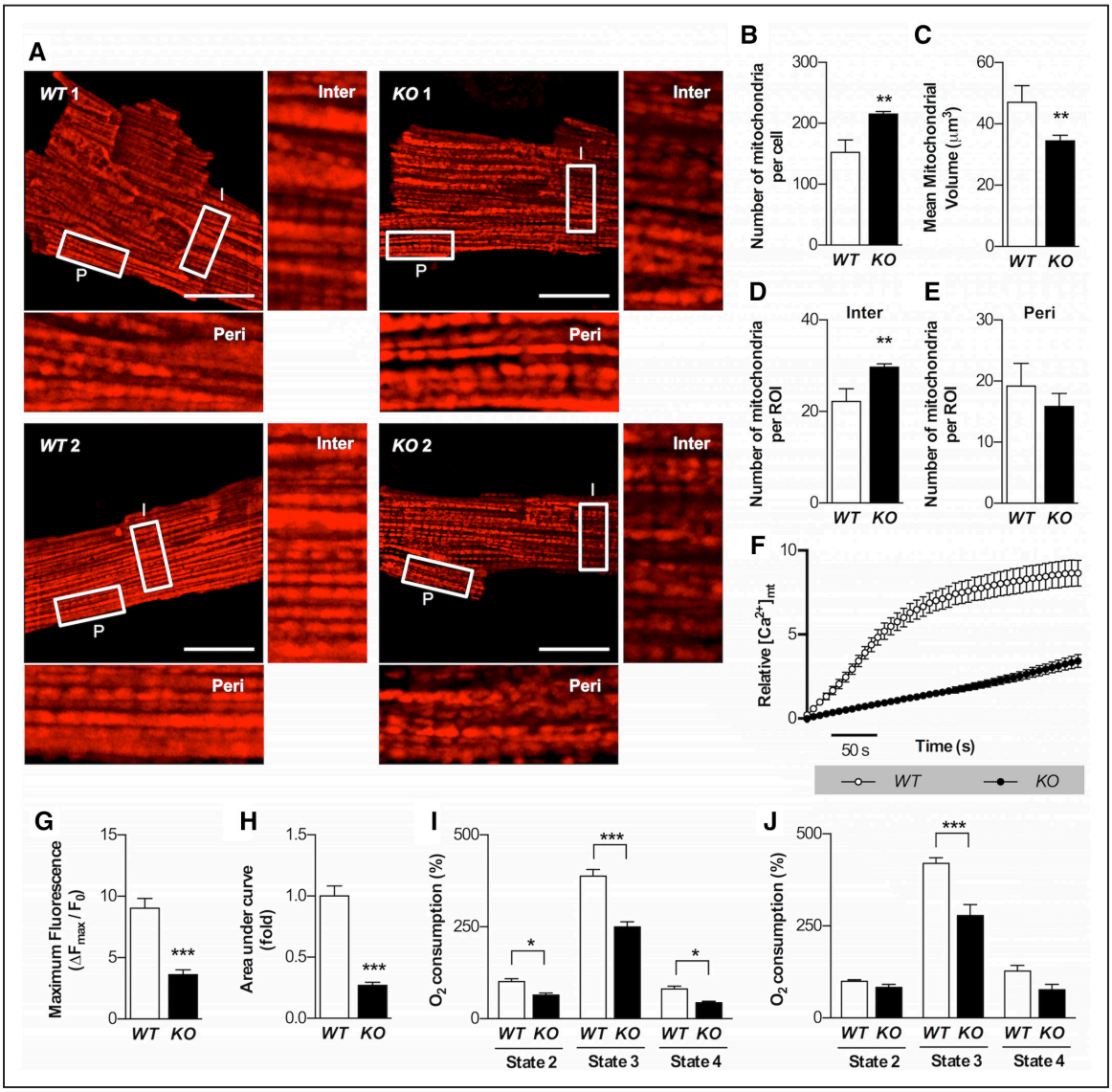

Figure 7. *Rcan1 KO* adult cardimyocytes show increased fission, decreased mitochondrial Ca^{2+} buffering capacity, and decreased mitochondrial function. A, Confocal Z stack reconstructions of wild-type (WT) and knockout (KO) adult mouse ventricular cardiomyocytes (AMVMs) stained with tetramethylrhodamine (TMRM; scale bar: 20 μm) were assessed for (**B**) the number of mitochondria per cell and (**C**) volume of individual mitochondria. Data are from 25 cells examined from 3 separate experiments. **D** and **E**, Interior (Inter) or peripheral (Peri) regions of interests from the images in **A** were assessed independently. **F**, Mitochondrial Ca^{2+} uptake in permeabilized AMVM stained with Rhod2. **G**, Quantification of *F* and (**H**) area under the curve during 300 s. Data are from 50 cells examined in 3 separate experiments. Oxygen consumption of permeabilized AMVMs using (**I**) pyruvate and (**J**) glutamate as substrates. n=4 from 3 different mice in each group. Mean±SEM; **P*<0.05, ***P*<0.01, ****P*<0.001. RCAN1 indicates regulator of calcineurin 1.

genotypes (Figure 8E). In the T21-iPSC, transcript and protein levels for RCAN1.1 were reduced to at, or below, those found in D21-iPSC (Figure 8E through 8G). This occurred without impacting markers of pluripotency as assessed by Western blot (Figure 8F) or quantitative reverse transcriptase polymerase chain reaction (Online Figure XI). RCAN1.4 protein was below the level of detection in these cells (Figure 8F). Remarkably, siRNA depletion of RCAN1.1 was sufficient to restore the mitochondrial network in the T21-iPSC to levels comparable to control siRNA-transfected D21-iPSC (Figure 8H through 8J). The rate of O_2 consumption in T21-iPSC was likewise restored to that measured in D21-iPSC (Figure 8K). Taken together, these data suggest that increased dosage of *RCAN1* may underlie a fundamental increase in mitochondrial fusion in the setting of trisomy 21 but may come at the cost of compromised coupling efficiency and reduced respiratory reserve.

Discussion

Mitochondrial metabolism and function play an important role in human health, disease, and aging. This is particularly true in highly oxidative organs such as the heart and brain where mitochondrial dysfunction is often a prominent feature of disease-related decline. In the setting of reperfusion injury after acute MI or stroke, mitochondria are the source of fundamental signals mediating cellular survival and death. In the context of RCAN1 deficiency, cardiac and neuronal damage after I/R is greater in *Rcan1-KO* mice, and forced expression in either

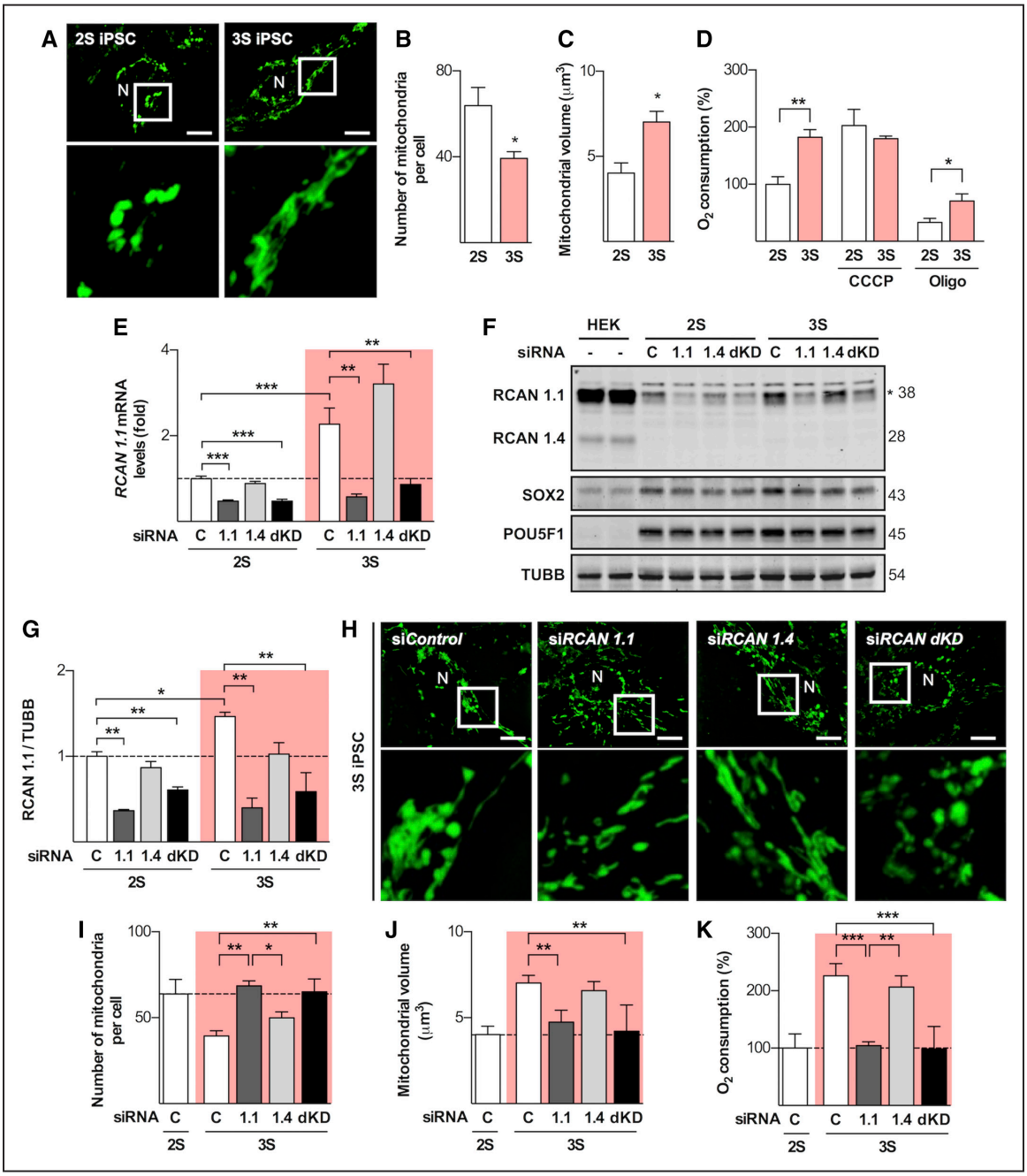

Figure 8. Trisomic induced pluripotent stem cell (iPSC) from individuals with Down syndrome have a more fused mitochondrial network and increased O_2 consumption. A, Disomic D21-iPSC (2S) and Trisomic T21-iPSC (3S) were stained with Mitotracker green and then analyzed by confocal microscopy to reconstruct the mitochondrial network. Representative images are provided from the D21-iPSC line No. 409 (2S) and the T21-iPSC line No. 416 (3S). Identical results were obtained from independent lines No. 406 (2S) and No. 419 (3S) (scale bar: 10 μm). **B**, Trisomic T21-iPSC contained fewer (**C**) and larger mitochondria compared with disomic D21-iPSC. Data are from 25 cells in 3 independent experiments. **D**, O_2 consumption rate was higher in T21-iPSC than in D21-iPSC. Maximal capacity and proton leak were assessed by adding oligomycin (Oligo; 50 nmol/L) or carbonyl cyanide *m*-chlorophenylhydrazone (CCCP; 200 nmol/L), respectively (n=5). **E**, Transcript levels for exon 1 isoform of RCAN1 (RCAN1.1) were higher in T21-iPSC than in D21-iPSC. Human-specific siRNAs targeting each of the RCAN1 isoforms were used to deplete endogenous RCAN1 from both lines and changes in endogenous *RCAN1.1* transcripts quantified by qPCR (n=4). **F**, The siRNA-depleted iPSC were analyzed by Western blot for RCAN1, SOX2, POU5F1, and TUBB proteins. HEK293 cells were used as controls. **G**, Densitometry was used to quantify RCAN1.1 protein levels in *F* normalized to TUBB (n=4). **H**, Trisomic T21-iPSC were depleted of RCAN1.1 and RCAN1.4, individually and in combination (dKD), and then stained for analysis of the mitochondrial network (scale bar: 10 μm). **I**, Depletion of RCAN1.1 alone or in combination with RCAN1.4 (dKD) increased mitochondrial number, (**J**) reduced average mitochondrial size, and (**K**) reduced basal reactive oxygen species (ROS) generation to levels (n=5). Mean±SEM; **P*<0.05, ***P*<0.01, ****P*<0.001. POU5F1 indicates POU class 5 homeobox; RCAN1, regulator of calcineurin 1; SOX2, SRY-box 2; and TUBB, β-tubulin.

cardiomyocytes or neurons can confer protection.[21–23,42] Here, we provide evidence that altering the levels of RCAN1 has a direct impact on mitochondrial dynamics. Based on these findings, we propose that the following cascade of events underlies the increase in sensitivity to reperfusion damage: In the absence of inhibition by RCAN1, increased CN activity promotes DRP1-mediated mitochondrial fission. The increase in fission decreases $\Delta\Psi_m$ and metabolic activity, lowering the capacity for mitochondrial Ca^{2+} uptake. Our studies suggest that, as a consequence, buffering of cytosolic Ca^{2+} is reduced, thereby, increasing CAPN-mediated damage after reperfusion. Although both cytosolic and mitochondrial localized CAPN can cause cellular damage, in the context of RCAN1 deficiency, the relevant pool, or pools, of CAPN are most likely cytosolic (Online Figure XII).

The reduction in OPA1 protein levels seen in RCAN1-depleted NRVMs is consistent with lower $\Delta\Psi_m$, as decreased membrane potential promotes OPA1 cleavage and degradation. Because of OPA1's role in mitochondrial fusion, the decline in OPA1 abundance may further shift the mitochondrial population toward fission in RCAN1-deficient cells. An increase in PINK1 protein is likewise consistent with reduced $\Delta\Psi_m$ as membrane potential is required for translocation of PINK1 into the mitochondrial matrix for subsequent degradation. Activation of PINK1 can initiate tagging of mitochondria for degradation via mitophagy. However, we saw no reduction in total mitochondrial mass in RCAN1-depleted cells, suggesting that the increase in PINK1 was either not sufficient to increase mitochondrial degradation or that an increase in mitochondrial biogenesis compensated for increased catabolism.

ROS generation during reperfusion is a well-documented mediator of I/R damage. However, the decrease in basal ROS activity and decline in maximal ETC capacity in the RCAN1-depleted NRVMs (Figure 3) would suggest that ROS-mediated damage may not be the primary mechanism mediating increased I/R sensitivity in culture. That does not preclude a mechanism involving elevated ROS in the context of the working heart and neurons where energetic demands might drive an increase in mitochondrial content to compensate for the decline in mitochondrial efficiency.

Our studies suggest that RCAN1.1 is the primary isoform impacting mitochondrial dynamics and function. However, in our experiments, the protein levels following *Ad-hRCAN1.1* infection were an order of magnitude higher than for *Ad-hRCAN1.4* (Online Figure VIIC and VIID and VIIIC and VIIID), thus, limiting the ability to draw definitive conclusions regarding isoform specificity based on the adenoviral complementation studies. The 2 isoforms are comparable in their ability to inhibit CN in biochemical assays, although some isoform-specific properties have been reported in vivo. For instance, we recently demonstrated an isoform-specific role for RCAN1.4 in the process of VEGF receptor internalization.[43]

In our studies, forced expression of RCAN1.1 was sufficient to increase mitochondrial fusion and confer protection from sI/R to both RCAN1.1-depleted and control siRNA-transfected NRVMs (Figure 6). Although overexpression using adenoviruses increased RCAN1.1 levels well over those of the endogenous protein, the studies comparing trisomic T21-iPSC to disomic D21-iPSC demonstrate that modest changes in RCAN1 levels can have a meaningful impact on mitochondrial dynamics and function. Altered mitochondrial function and increased oxidative stress have long been associated with DS.[16] Although there is no universal agreement regarding morphological changes to the mitochondrial network in trisomic tissues, an increase in mitochondrial ROS generation is widely reported and would be consistent with the increased fusion observed in the T21-iPSC. In addition, increased mitochondrial Ca^{2+} levels are documented in both heart and cultured fibroblasts from DS fetuses.[44] Our findings point toward a mechanism through which increased RCAN1 dosage could underlie these changes.

In the context of I/R damage, these studies suggest that increased fusion protects cardiomyocytes by reducing the extent of CAPN activation after reperfusion. However, a sustained increase in fusion may also have negative consequences. Indeed, although an increase in $\Delta\Psi_m$ increased the capacity for ATP generation, it also increased the capacity for ROS generation, thereby, increasing the potential for cellular damage. Sustained fusion could also slow the process of mitochondrial turnover and repair. Over time, these 2 mechanisms would act to fuel the generation and accumulation of damaged mitochondrial components. This may be the underlying cause of the increase in uncoupling observed in both trisomic T21-iPSC and NRVMs infected with *Ad-hRCAN1.1*. Alternative explanations for the decline in coupling efficiency are activation of protective compensatory mechanisms or a direct impact of RCAN1 on mitochondrial coupling. Along these lines, it is relevant to note that RCAN has been reported to interact both directly[45] and indirectly[46] with the adenine nucleotide translocase, a protein which can act to uncouple the inner mitochondrial membrane proton gradient.[47]

Transgenic overexpression of *RCAN1* is reported to increase mitochondrial ROS in both neurons and pancreatic islets.[48,49] Under normal glucose conditions, $\Delta\Psi_m$ is elevated in islets overexpressing *RCAN1* but is depressed in response to elevated glucose.[50] Thus, changes mediated by RCAN1 may be context dependent. As an example, we recently showed that brain-specific overexpression of *RCAN1.1* caused age-dependent cognitive impairments similar to early-onset dementia seen in individuals with DS.[51] Mitochondrial ROS and the number of large, globular mitochondria increased in the brains of these animals; consistent with the mechanism we report here, however, there was also an accompanying, age-dependent decline in DRP1 phosphorylation, not predicted by our model. We postulate that this may be the combined outcome of primary effects, cumulative damage, and compensatory mechanisms. The mitochondrial network of trisomic Ts21-iPSC may more closely represent primary fundamental differences in mitochondria dynamics because iPSC are predominately glycolytic and, therefore, not yet impacted by functional selection as might occur in the setting of an intact animal or even differentiated cell types in culture.

Taken together, our studies indicate a dose-dependent response of the mitochondrial network to changes in the availability of RCAN1. RCAN1 insufficiency favors fission, thereby, reducing mitochondrial metabolic activity and capacity for mitochondrial Ca^{2+} uptake. In the case of RCAN1-depleted NRVM, this increases vulnerability to sI/R damage

because of increased CAPN-mediated damage on reperfusion. Although forced RCAN1.1 expression is sufficient to promote fusion and increase metabolic activity, in the setting of trisomy 21, this may occur at the cost of compromising coupling efficiency and loss of metabolic flexibility. Our findings highlight the need for maintaining appropriate RCAN1 levels and suggest a mechanism through which increased dosage of the RCAN1 locus in DS may impact human health at the fundamental level of mitochondrial dynamics.

Acknowledgments

We thank members of the Rothermel, Parra, Hill, and Lavandero laboratories for stimulating discussions and support. We also thank Ingenio Bravo for crafting of figures and Christi Hull and Sebastián Leiva for their excellent technical assistance.

Sources of Funding

This work was supported by FONDECYT (11150282 to V. Parra, 1150887 to Z. Pedrozo, and 1161156 to S. Lavandero); FONDAP (15130011 to V. Parra, Z. Pedrozo, and S. Lavandero); PAI Insertion Program, CONICYT (grant 79150007 to V. Parra and S. Lavandero); the National Institutes of Health (NIH; HL-120732, HL-126012, and HL-128215 to J.A. Hill; HL097768 and HL072016 to B.A. Rothermel; PCBC JS 2014/3 01 to V. Parra and J.W. Schneider); American Heart Association (AHA; 13POST16520009 to V. Parra; 16POST30680016 to F. Altamirano; 11POST7950051 to D. Rotter; and 14SFRN20510023 and 14SFRN20670003 to J.A. Hill); Fondation Leducq (11CVD04 to J.A. Hill); and Cancer Prevention and Research Institute of Texas (RP110486P3 to J.A. Hill).

Disclosures

None.

References

1. Mozaffarian D, Benjamin EJ, Go AS, et al; American Heart Association Statistics Committee and Stroke Statistics Subcommittee. Heart disease and stroke statistics–2015 update: a report from the American Heart Association. *Circulation*. 2015;131:e29–e322. doi: 10.1161/CIR.0000000000000152.
2. Halestrap AP. A pore way to die: the role of mitochondria in reperfusion injury and cardioprotection. *Biochem Soc Trans*. 2010;38:841–860. doi: 10.1042/BST0380841.
3. Di Lisa F, Canton M, Carpi A, Kaludercic N, Menabò R, Menazza S, Semenzato M. Mitochondrial injury and protection in ischemic pre- and postconditioning. *Antioxid Redox Signal*. 2011;14:881–891. doi: 10.1089/ars.2010.3375.
4. Ong SB, Subrayan S, Lim SY, Yellon DM, Davidson SM, Hausenloy DJ. Inhibiting mitochondrial fission protects the heart against ischemia/reperfusion injury. *Circulation*. 2010;121:2012–2022. doi: 10.1161/CIRCULATIONAHA.109.906610.
5. Vásquez-Trincado C, García-Carvajal I, Pennanen C, Parra V, Hill JA, Rothermel BA, Lavandero S. Mitochondrial dynamics, mitophagy and cardiovascular disease. *J Physiol*. 2016;594:509–525. doi: 10.1113/JP271301.
6. Santel A, Frank S. Shaping mitochondria: the complex posttranslational regulation of the mitochondrial fission protein DRP1. *IUBMB Life*. 2008;60:448–455. doi: 10.1002/iub.71.
7. Otera H, Ishihara N, Mihara K. New insights into the function and regulation of mitochondrial fission. *Biochim Biophys Acta*. 2013;1833:1256–1268. doi: 10.1016/j.bbamcr.2013.02.002.
8. Cribbs JT, Strack S. Reversible phosphorylation of Drp1 by cyclic AMP-dependent protein kinase and calcineurin regulates mitochondrial fission and cell death. *EMBO Rep*. 2007;8:939–944. doi: 10.1038/sj.embor.7401062.
9. Li HC, Chan WW. Activation of brain calcineurin towards proteins containing Thr(P) and Ser(P) by Ca2+, calmodulin, Mg2+ and transition metal ions. *Eur J Biochem*. 1984;144:447–452.
10. Letavernier E, Zafrani L, Perez J, Letavernier B, Haymann JP, Baud L. The role of calpains in myocardial remodelling and heart failure. *Cardiovasc Res*. 2012;96:38–45. doi: 10.1093/cvr/cvs099.
11. Garcia-Dorado D, Ruiz-Meana M, Inserte J, Rodriguez-Sinovas A, Piper HM. Calcium-mediated cell death during myocardial reperfusion. *Cardiovasc Res*. 2012;94:168–180. doi: 10.1093/cvr/cvs116.
12. Molkentin JD, Lu JR, Antos CL, Markham B, Richardson J, Robbins J, Grant SR, Olson EN. A calcineurin-dependent transcriptional pathway for cardiac hypertrophy. *Cell*. 1998;93:215–228.
13. Fuentes JJ, Genescà L, Kingsbury TJ, Cunningham KW, Pérez-Riba M, Estivill X, de la Luna S. DSCR1, overexpressed in Down syndrome, is an inhibitor of calcineurin-mediated signaling pathways. *Hum Mol Genet*. 2000;9:1681–1690.
14. Rothermel B, Vega RB, Yang J, Wu H, Bassel-Duby R, Williams RS. A protein encoded within the Down syndrome critical region is enriched in striated muscles and inhibits calcineurin signaling. *J Biol Chem*. 2000;275:8719–8725.
15. Fuentes JJ, Pritchard MA, Planas AM, Bosch A, Ferrer I, Estivill X. A new human gene from the Down syndrome critical region encodes a proline-rich protein highly expressed in fetal brain and heart. *Hum Mol Genet*. 1995;4:1935–1944.
16. Helguera P, Seiglie J, Rodriguez J, Hanna M, Helguera G, Busciglio J. Adaptive downregulation of mitochondrial function in Down syndrome. *Cell Metab*. 2013;17:132–140. doi: 10.1016/j.cmet.2012.12.005.
17. Yang J, Rothermel B, Vega RB, Frey N, McKinsey TA, Olson EN, Bassel-Duby R, Williams RS. Independent signals control expression of the calcineurin inhibitory proteins MCIP1 and MCIP2 in striated muscles. *Circ Res*. 2000;87:E61–E68.
18. Rothermel BA, McKinsey TA, Vega RB, Nicol RL, Mammen P, Yang J, Antos CL, Shelton JM, Bassel-Duby R, Olson EN, Williams RS. Myocyte-enriched calcineurin-interacting protein, MCIP1, inhibits cardiac hypertrophy in vivo. *Proc Natl Acad Sci USA*. 2001;98:3328–3333. doi: 10.1073/pnas.041614798.
19. van Rooij E, Doevendans PA, Crijns HJ, Heeneman S, Lips DJ, van Bilsen M, Williams RS, Olson EN, Bassel-Duby R, Rothermel BA, De Windt LJ. MCIP1 overexpression suppresses left ventricular remodeling and sustains cardiac function after myocardial infarction. *Circ Res*. 2004;94:e18–e26. doi: 10.1161/01.RES.0000118597.54416.00.
20. Hill JA, Rothermel B, Yoo KD, Cabuay B, Demetroulis E, Weiss RM, Kutschke W, Bassel-Duby R, Williams RS. Targeted inhibition of calcineurin in pressure-overload cardiac hypertrophy. Preservation of systolic function. *J Biol Chem*. 2002;277:10251–10255. doi: 10.1074/jbc.M110722200.
21. Rotter D, Grinsfelder DB, Parra V, Pedrozo Z, Singh S, Sachan N, Rothermel BA. Calcineurin and its regulator, RCAN1, confer time-of-day changes in susceptibility of the heart to ischemia/reperfusion. *J Mol Cell Cardiol*. 2014;74:103–111. doi: 10.1016/j.yjmcc.2014.05.004.
22. Sobrado M, Ramirez BG, Neria F, Lizasoain I, Arbones ML, Minami T, Redondo JM, Moro MA, Cano E. Regulator of calcineurin 1 (Rcan1) has a protective role in brain ischemia/reperfusion injury. *J Neuroinflammation*. 2012;9:48. doi: 10.1186/1742-2094-9-48.
23. Sanna B, Brandt EB, Kaiser RA, Pfluger P, Witt SA, Kimball TR, van Rooij E, De Windt LJ, Rothenberg ME, Tschop MH, Benoit SC, Molkentin JD. Modulatory calcineurin-interacting proteins 1 and 2 function as calcineurin facilitators in vivo. *Proc Natl Acad Sci USA*. 2006;103:7327–7332. doi: 10.1073/pnas.0509340103.
24. Parra V, Eisner V, Chiong M, Criollo A, Moraga F, Garcia A, Härtel S, Jaimovich E, Zorzano A, Hidalgo C, Lavandero S. Changes in mitochondrial dynamics during ceramide-induced cardiomyocyte early apoptosis. *Cardiovasc Res*. 2008;77:387–397. doi: 10.1093/cvr/cvm029.
25. Parra V, Verdejo HE, Iglewski M, et al. Insulin stimulates mitochondrial fusion and function in cardiomyocytes via the Akt-mTOR-NFκB-Opa-1 signaling pathway. *Diabetes*. 2014;63:75–88. doi: 10.2337/db13-0340.
26. Pennanen C, Parra V, López-Crisosto C, Morales PE, Del Campo A, Gutierrez T, Rivera-Mejías P, Kuzmicic J, Chiong M, Zorzano A, Rothermel BA, Lavandero S. Mitochondrial fission is required for cardiomyocyte hypertrophy mediated by a Ca2+-calcineurin signaling pathway. *J Cell Sci*. 2014;127:2659–2671. doi: 10.1242/jcs.139394.
27. Parra V, Verdejo H, del Campo A, Pennanen C, Kuzmicic J, Iglewski M, Hill JA, Rothermel BA, Lavandero S. The complex interplay between mitochondrial dynamics and cardiac metabolism. *J Bioenerg Biomembr*. 2011;43:47–51. doi: 10.1007/s10863-011-9332-0.
28. Wang W, Karamanlidis G, Tian R. Novel targets for mitochondrial medicine. *Sci Transl Med*. 2016;8:326rv3. doi: 10.1126/scitranslmed.aac7410.

29. Jin SM, Lazarou M, Wang C, Kane LA, Narendra DP, Youle RJ. Mitochondrial membrane potential regulates PINK1 import and proteolytic destabilization by PARL. *J Cell Biol*. 2010;191:933–942. doi: 10.1083/jcb.201008084.
30. Eisner V, Parra V, Lavandero S, Hidalgo C, Jaimovich E. Mitochondria fine-tune the slow Ca(2+) transients induced by electrical stimulation of skeletal myotubes. *Cell Calcium*. 2010;48:358–370. doi: 10.1016/j.ceca.2010.11.001.
31. Eisner V, Csordás G, Hajnóczky G. Interactions between sarco-endoplasmic reticulum and mitochondria in cardiac and skeletal muscle - pivotal roles in Ca^{2+} and reactive oxygen species signaling. *J Cell Sci*. 2013;126:2965–2978. doi: 10.1242/jcs.093609.
32. Hernando V, Inserte J, Sartório CL, Parra VM, Poncelas-Nozal M, Garcia-Dorado D. Calpain translocation and activation as pharmacological targets during myocardial ischemia/reperfusion. *J Mol Cell Cardiol*. 2010;49:271–279. doi: 10.1016/j.yjmcc.2010.02.024.
33. Sorimachi H, Ono Y. Regulation and physiological roles of the calpain system in muscular disorders. *Cardiovasc Res*. 2012;96:11–22. doi: 10.1093/cvr/cvs157.
34. Inserte J, Hernando V, Garcia-Dorado D. Contribution of calpains to myocardial ischaemia/reperfusion injury. *Cardiovasc Res*. 2012;96:23–31. doi: 10.1093/cvr/cvs232.
35. Pedrozo Z, Sánchez G, Torrealba N, Valenzuela R, Fernández C, Hidalgo C, Lavandero S, Donoso P. Calpains and proteasomes mediate degradation of ryanodine receptors in a model of cardiac ischemic reperfusion. *Biochim Biophys Acta*. 2010;1802:356–362. doi: 10.1016/j.bbadis.2009.12.005.
36. Ali MA, Stepanko A, Fan X, Holt A, Schulz R. Calpain inhibitors exhibit matrix metalloproteinase-2 inhibitory activity. *Biochem Biophys Res Commun*. 2012;423:1–5. doi: 10.1016/j.bbrc.2012.05.005.
37. Chang KT, Shi YJ, Min KT. The Drosophila homolog of Down's syndrome critical region 1 gene regulates learning: implications for mental retardation. *Proc Natl Acad Sci USA*. 2003;100:15794–15799. doi: 10.1073/pnas.2536696100.
38. Ermak G, Harris CD, Davies KJ. The DSCR1 (Adapt78) isoform 1 protein calcipressin 1 inhibits calcineurin and protects against acute calcium-mediated stress damage, including transient oxidative stress. *FASEB J*. 2002;16:814–824. doi: 10.1096/fj.01-0846com.
39. Crawford DR, Leahy KP, Abramova N, Lan L, Wang Y, Davies KJ. Hamster adapt78 mRNA is a Down syndrome critical region homologue that is inducible by oxidative stress. *Arch Biochem Biophys*. 1997;342:6–12. doi: 10.1006/abbi.1997.0109.
40. Leahy KP, Crawford DR. adapt78 protects cells against stress damage and suppresses cell growth. *Arch Biochem Biophys*. 2000;379:221–228. doi: 10.1006/abbi.2000.1897.
41. Maclean GA, Menne TF, Guo G, Sanchez DJ, Park I-H, Daley GQ, Orkin SH. Altered hematopoiesis in trisomy 21 as revealed through in vitro differentiation of isogenic human pluripotent cells. *Proc Natl Acad Sci USA*. 2012;109:17567–17572.
42. Brait VH, Martin KR, Corlett A, Broughton BR, Kim HA, Thundyil J, Drummond GR, Arumugam TV, Pritchard MA, Sobey CG. Overexpression of DSCR1 protects against post-ischemic neuronal injury. *PLoS One*. 2012;7:e47841. doi: 10.1371/journal.pone.0047841.
43. Alghanem AF, Wilkinson EL, Emmett MS, Aljasir MA, Holmes K, Rothermel BA, Simms VA, Heath VL, Cross MJ. RCAN1.4 regulates VEGFR-2 internalisation, cell polarity and migration in human microvascular endothelial cells. *Angiogenesis*. 2017;20:341–358. doi: 10.1007/s10456-017-9542-0.
44. Piccoli C, Izzo A, Scrima R, et al. Chronic pro-oxidative state and mitochondrial dysfunctions are more pronounced in fibroblasts from Down syndrome foeti with congenital heart defects. *Hum Mol Genet*. 2013;22:1218–1232. doi: 10.1093/hmg/dds529.
45. Chang KT, Min KT. Drosophila melanogaster homolog of Down syndrome critical region 1 is critical for mitochondrial function. *Nat Neurosci*. 2005;8:1577–1585. doi: 10.1038/nn1564.
46. Jiang H, Zhang C, Tang Y, Zhao J, Wang T, Liu H, Sun X. The regulator of calcineurin 1 increases adenine nucleotide translocator 1 and leads to mitochondrial dysfunctions. *J Neurochem*. 2017;140:307–319. doi: 10.1111/jnc.13900.
47. Azzu V, Brand MD. The on-off switches of the mitochondrial uncoupling proteins. *Trends Biochem Sci*. 2010;35:298–307. doi: 10.1016/j.tibs.2009.11.001.
48. Peiris H, Raghupathi R, Jessup CF, Zanin MP, Mohanasundaram D, Mackenzie KD, Chataway T, Clarke JN, Brealey J, Coates PT, Pritchard MA, Keating DJ. Increased expression of the glucose-responsive gene, RCAN1, causes hypoinsulinemia, β-cell dysfunction, and diabetes. *Endocrinology*. 2012;153:5212–5221. doi: 10.1210/en.2011-2149.
49. Peiris H, Dubach D, Jessup CF, Unterweger P, Raghupathi R, Muyderman H, Zanin MP, Mackenzie K, Pritchard MA, Keating DJ. RCAN1 regulates mitochondrial function and increases susceptibility to oxidative stress in mammalian cells. *Oxid Med Cell Longev*. 2014;2014:520316. doi: 10.1155/2014/520316.
50. Peiris H, Duffield MD, Fadista J, et al. A syntenic cross species aneuploidy genetic screen links RCAN1 expression to β-cell mitochondrial dysfunction in type 2 diabetes. *PLoS Genet*. 2016;12:e1006033. doi: 10.1371/journal.pgen.1006033.
51. Wong H, Levenga J, Cain P, Rothermel B, Klann E, Hoeffer C. RCAN1 overexpression promotes age-dependent mitochondrial dysregulation related to neurodegeneration in Alzheimer's disease. *Acta Neuropathol*. 2015;130:829–843. doi: 10.1007/s00401-015-1499-8.

Circulation Research
JOURNAL OF THE AMERICAN HEART ASSOCIATION

Down Syndrome Critical Region 1 Gene, *Rcan1*, Helps Maintain a More Fused Mitochondrial Network

Valentina Parra, Francisco Altamirano, Carolina P. Hernández-Fuentes, Dan Tong, Victoriia Kyrychenko, David Rotter, Zully Pedrozo, Joseph A. Hill, Verónica Eisner, Sergio Lavandero, Jay W. Schneider and Beverly A. Rothermel

Circ Res. 2018;122:e20-e33; originally published online January 23, 2018;
doi: 10.1161/CIRCRESAHA.117.311522
Circulation Research is published by the American Heart Association, 7272 Greenville Avenue, Dallas, TX 75231

Print ISSN: 0009-7330. Online ISSN: 1524-4571

Supplemental Materials

Online Methods:

Reagents. Details of antibody sources, dilution, and validation can be found in Online Table I. Matrigel membrane matrix was purchased from Thermo Fischer Scientific (Waltham, MA, USA). Mitotracker green FM, Rhod-FF AM, Rhod2 AM, Fura-2, Fluo-4, Tetramethylrhodamine methyl ester perchlorate (TMRM), MitoSOX™, Lipofectamine® RNAiMax, BAPTA AM, Optimem®, FBS and KnockOut DMDM/F12 were from Invitrogen (Eugene, OR, USA). Anti-DRP1 antibody (611112) was from Becton-Dickinson (San Jose, CA, USA) and Anti-POU5F1 (SC-5279) was from Santa Cruz Biotechnology (Dallas, TX, USA). FK506 was purchased from ENZO Life Sciences (Farmingdale, NY, USA). MDL 28170 and PD 150606 were from Tocris Bioscience (Bristol, UK). Carbonyl cyanide m-chlorophenylhydrazone (CCCP), Dihydrorhodamine 123, Oligomycin, Forskolin, E-64D, DMEM, M199 medium were from Sigma-Aldrich Corp. (St. Louis, MO, USA). mTESR1 was purchased in Stemcell Technologies (Vancouver, Canada) and Y27632 in Selleck Chemicals (Houston, TX, USA). Mitochondrial division inhibitor (Mdivi-1), Ruthenium Red (RuRed) and all other inorganic compounds, salts and solvents were from Merck (Darmstadt, Germany). Protein assay reagents were from Bio-Rad (Hercules, CA, USA). Generation of the *Ad-hRCAN1.1* and *Ad-hRCAN1.4* adenovirus (both Ad5 serotype) was described previously.[1,2] Cardiomyocytes were transduced with adenoviral vectors at a multiplicity of infection (MOI) up to 1,000, 48 h before analysis or sI/R. A β-Gal adenovirus was used as a control at equivalent MOIs.

Animals. C57BL/6:129 mixed background, male, wild type (*WT*) and *Rcan1 KO* mice were raised and maintained in ventilated chambers as previously described.[3] The environment was maintained at 22°C with a 12-h light/12-h dark cycle. All animal procedures were carried out with the oversight and approval of the UT Southwestern Medical Center Institutional Animal Care and Use Committee and conformed to the current Guide for the Care and Use of Laboratory Animals, published by the National Institutes of Health. For electron microscopy, tissue of the interventricular septum of the heart of 8-week-old male littermate *WT* and *KO* mice were dissected.

Culture of cardiomyocytes and simulated I/R. NRVM were isolated from 1- to 2-day-old Sprague-Dawley rat pups as previously described.[4] Cells were grown for 48 h in DMEM:M199 (4:1), 5% FBS, with BrdU plus antibiotics, then transfected with respective siRNAs. 48 h after transfection, media was changed to ischemia-mimicking solutions containing 5 mM HEPES, 10 mM 2-deoxy-D-glucose, 139 mM NaCl, 12 mM KCl, 0.5 mM $MgCl_2$, 1.3 mM $CaCl_2$, and 20 mM lactic acid, pH 6.2, then incubated under 100% nitrogen (O_2 < 1%) at 37 °C for 6 h. The cultures were then returned to normal culture conditions for 12 h, DMEM/M199 (4:1), 5% FBS; 37 °C ambient air, 5% CO_2. Release of lactate dehydrogenase (LDH) into the media and remaining in the cells was measured using the Promega CytoTox 96® kit (Madison, Wi, USA). The ratio of released LDH to total LDH was used as a relative measure of cell death. FK507 and Mdivi-1 were added to the media during the siRNA transfection, whereas CAPN inhibitors (10 μM E-64D, 10 μM MDL 28170 and 10 μM PD 150606), 1 μM BAPTA and 10 μM RuRed were added 30 min prior to ischemia.

Cardiomyocyte transfection. Small interfering RNAs (siRNA) for *Rcan1.1* and/or *Rcan1.4* (Dharmacon ON-TARGETplus; Lafayette, CO, USA), CAPN (*Capn1* and *Capn2*) and negative control (Mission, Sigma-Aldrich Corp., St Louis, MO) were used following the manufacturer's instructions. Following isolation, NRVM were cultured for 48 h, prior to transfected with siRNAs at a concentration of 50 nM with Lipofectamine® RNAiMAX (Invitrogen, Carlsbad, CA). After 6 h incubation in Optimem®, the medium was removed and replaced with 5% FBS in DMEM/M199. Changes in *Rcan1* or *Capn 1/2* protein and/or transcript levels were assessed 48 h post-transfection. The siRNAs used for knockdown experiments were as follows: negative control, catalog number SIC001; rat *Rcan1.1*, sense

(5"-UGGAGGAGGUGGAUCUGCAUU-3"), antisense (5"-UGCAGAUCCACCUCCUCCAUU-3"); rat *Rcan1.4*, sense (5"-GAUGAUGUCUUCAGCGAAAUU-3"), antisense (5"-UUUCGCUGAAGACAUCAUCUU-3"); rat *Capn1*, 1a sense (5"-GUUGUGACCUUUGAUCUAU-3"), antisense (5"-AUAGAUCAAAGGUCACAAC-3"); rat *Capn2*, 2a sense (5"-GAACGUACGGGAACAUUUA-3"), antisense (5"-UAAAUGUUCCCGUACGUUC-3"). Average depletion of RCAN1.1 and RCAN1.4 was 90% ($P < 0.001$) and 84% ($P < 0.001$) respectively (Online Figure IA). An unrelated siRNA capable of depleting both *Rcan1* transcripts was obtained from Life Technologies (*Rcan1* rat stealth siRNA, catº RSS332844). RCAN1 depletion using this alternative siRNA corroborated the results obtained with the isoform-specific siRNAs (Online Figure IB-F). The *Capn* siRNAs used in our studies were selected from a group of siRNAs targeting either *Capn1* or *2* that were screened in various combinations for efficiency of knock down in Online Figure IVE-F and as previously described.[5] A mixture combining siRNA 1a (targeting *Capn1*) and 2a (targeting *Capn2*) was used in all subsequent experiments.

Isolation of Adult mouse cardiomyocytes (AMVM). Adult cardiomyocytes were prepared as previously described.[6] Briefly, hearts were perfused retrograde with perfusion media (PM) (123 mM NaCl, 4.7 mM KCl, 0.6 mM KH_2PO_4, 0.6 mM Na_2HPO_4, 1.2 mM $MgSO_4$, 10 mM HEPES, 22 mM $NaHCO_3$, 30 mM taurine, 10 mM 2,3-butanedione monoxime, and 5.5 mM glucose, pH 7.4) for 2 min (2-4 mL/min) and then switched to PM supplemented with 0.025 mg/mL Liberase TM (Roche) and 0.025% Trypsin for 14 min. After digestion, ventricles were dissected and mechanically dissociated in PM using forceps and pipetting. Cell yield was approximately 80-90% viable, and only quiescent cardiomyocytes with clear and defined striations were used in this study. Cells were used immediately for experiments and kept in PM media with 50 μM Ca^{2+} and Matrigel was used to promote cell adhesion to MatTek 35 mm dishes.

Induced iPSC and MEF. Human Trisomy 21 iPSC (T21-iPSC) and their isogenic disomic derivatives (D21-iPDC) were obtained through the NHLBI Progenitor Cell Biology Consortium (https://progenitorcells.org/) and the specifics of their derivation were described previously.[7] iPSC were grown in mTESR1 medium and passaged non-enzymatically using 0.5 M EDTA, pH 8.0. Y27632 10 μM was used during splitting to improve cell survival, split ratio reliability, and to reduce selective pressure. Cells were passaged at a 1 to 12-20 split ratio, mTESR medium was changed every day. At 60-80% confluence, cells were either passaged or used for experiments. For transfection, cells were grown in 35-mm plates and treated with Y27632 10 μM for 1 h, then exposed to 50 nM of human siRNA in 200 mL of Optimem®. After 20 min, culture volume was brought to 1 mL using mTESR medium. Cells were analysed 48 h later. The siRNAs targeting human *RCAN1* were as follows: *RCAN1.1*, sense (5"-GCUUCAUUGACUGCGAGAUU-3"), antisense (5"-UCUCGCAGUCAAUGAAGCUU-3"); *RCAN1.4*, sense (5"-AGUGAUAUCUUCAGCGAAAUU-3"), antisense (5"-UUUCGCUGAAGAUAUCACUUU-3"). MEF were isolated from *WT* and *Rcan1 KO* embryos using standard procedures.[8] MEF were cultured in DMEM 10% FBS plus 100 μM non-essential amino acids and 2 μM L-glutamine supplemented with 1% penicillin/streptomycin at 37ºC in a 5% CO_2 atmosphere. All the analyses described throughout this study were carried out at passages 4–5.

Transmission electron microscopy. Tissues and cells were fixed in 2.5% glutaraldehyde in sodium cacodylate buffer, embedded in 2% agarose, post-fixed in buffered 1% osmium tetroxide and stained in 2% uranyl acetate, dehydrated with an ethanol graded series and embedded in EMbed-812 resin. Thin sections were cut on an ultramicrotome and stained with 2% uranyl acetate and lead citrate. Images were acquired on a FEI Tecnai G2 Spirit electron microscope equipped with a LaB6 source and operating at 120 kV. Measurements of mitochondrial area, perimeter, circularity and mitochondrial density were made using the Multi measure ROI tool of ImageJ (National Institutes of Health) software.[9] Tissues were harvested at 10 AM, 4 hours into the animal's light cycle.

Analysis of the mitochondrial network. Cells were incubated for 30 min with Mitotracker green FM (400 nM) in the case of NRVMs or TMRM (10 μM for 10 min) for AMVMs and maintained in Krebs solution. Confocal image stacks were captured with a Zeiss LSM-5, Pascal 5 Axiovert 200 microscope, using LSM 5 3.2 image capture and analysis software and a Plan-Apochromat 63x/1.4 Oil DIC objective, as previously described.[9,10] Images were deconvolved with ImageJ and then Z-stacks of thresholded images were volume-reconstituted. The number and individual volume of each object (mitochondrion) were quantified using the ImageJ-3D object counter plugging with each detected mitochondria isolated from the different Z-stack planes. Each experiment was done at least three times and 16–25 cells per condition were quantified. An increase in mitochondrial volume and a decrease in the number of mitochondria were considered as a fusion criteria, whereas a decrease in mitochondrial volume and an increase in the number of mitochondria were considered as a fission criteria.[9-11] Histograms and density images were constructed using ImageJ as previously described.[9,12] For the analysis of the mitochondrial density and the generation of the intensity density heat map, we used the images directly generated by the ImageJ-3D object counter plugging and then manipulated de Lut Table in order to highlight the differences in density with a more suitable coloring pattern. To quantify changes in mitochondrial distribution we used radial profile analysis, as described previously.[12] Briefly, an algorithm for the ImageJ software was created to scan radial fluorescence and object distribution, measured from the center of the nucleus towards the plasma membrane in a full-angle mode (0-360°), as illustrated in Online Figure VA). Using this tool, we compared changes in the subcellular distribution of the mitochondrial network between control and RCAN1-depleted NRVM.

Fluorescence recovery after photobleaching. For fluorescence recovery after photobleaching (FRAP) measurements, cells were loaded with 200 nM TMRM for 30 min at 37°C in Krebs solution. TMRM was excited at 561 nm, and fluorescence emission was detected with a 650/710-emission filter. Bleaching of TMRM fluorescence was applied in an ~25 mm^2 square at randomly chosen regions, and fluorescence intensity was normalized to the intensity levels before and after bleaching.[10]

Subcellular fractionation. Mitochondrial and cytosolic fractions were obtained by differential centrifugation of cardiomyocyte homogenates using a Mitochondrial/Cytosol fractionation kit from Biovision Inc. (Milpitas, CA, USA). Briefly, cells were scraped, pelleted, and re-suspended in ice-cold cytosol extraction buffer. Cells were homogenized using a homogenizer with a tight fitting Teflon pestle. The homogenates were centrifuged (750 g, 10 min) to remove nuclei and unbroken cells, and supernatants were centrifuged (10,000 g, 25 min) to obtain a pellet highly enriched in mitochondria. The protein content was determined by Bradford's method. The purity of mitochondrial fraction, assessed by HSPA9 levels [10, 13] was 85%.

Western blot analysis. Cell and tissue total protein extracts were analysed as described previously.[10] Protein contents were normalized to TUBB or GAPDH. To assess the phosphorylation status of DRP1, total DRP1 was immunoprecipitated from total cell extracts overnight using 2 μg of anti-DRP1 antibody on 400 μg of total protein. DRP1 was precipitated with Sepharose beads conjugated to protein G (Santa Cruz, Dallas, TX, USA), resolved by SDS-PAGE and then phosphorylation was assessed with anti-phospho-DRP1 antibody.

ATP measurements. ATP content in cells was determined using a luciferin/luciferase-based assay (CellTiter-Glo Kit; Promega).

Flow cytometry analysis of mitochondrial membrane potential, mitochondrial mass and ROS. $\Delta\Psi_m$, mitochondrial mass, and ROS levels were measured after loading cardiomyocytes with TMRM (200 nM, 30 min; excitation/emission 543/560), MitoTracker Green FM (400 nM, 30 min; excitation/emission 488/530), MitoSox® (5 μM, 10 min; excitation/emission 510/580) or Dihydrorhodamine 123 (25 μM, 20 min; excitation/emission 510/530). Afterward, cells underwent trypsinization, and fluorescence was

assessed by flow cytometry with a FACScan system (Becton Dickinson, Franklin Lakes, NJ, U.S.A). CCCP (50 μM) and oligomycin (10 μM) for 30 min were used as positive and negative controls for the $\Delta\Psi_m$ measurements, whereas H_2O_2 (5 mM) was used as a positive control in the ROS assays.

Oxygen consumption. For NRVMs, oxygen consumption was measured using a fluorescence-based oxygen sensor (NeoFox, Ocean Optics, Dunedin, FL, USA) connected to a phase measurement system from the same company. The sensor was calibrated according to the manufacturer's instructions as previously described.[14] In the case of the adult mouse ventricular cardiomyocytes, AMVMs were isolated by enzymatic digestion. Cell numbers were carefully counted using a hemocytometer. Only cells with sharp borders and clear striations were selected. Briefly, $1x10^4$ cardiomyocytes were incubated in a solution containing KMES 60 mM, $MgCl_2$ 3 mM, KH_2PO_4 10 mM, Hepes 20 mM, Taurine 20 mM, Mannitol 110 mM, EGTA 0.5 mM, and DTT 0.3 mM (PH 7.1) at 37º, and permeabilized with saponin (50 ng/ml) for 5 minutes before substrates were added. To measure complex I mediated OCR, glutamate (10 mM) and malate (5mM) were added. State3 respiration was activated by adding ADP (2.5 mM), whereas state4 respiration was measured after adding oligomycin (2 μM). For the measuring of pyrvuate mediated OCR, 0.1 mM of pyruvate was added to each experiment. AMVMs were isolated at the beginning of the animal's light cycle, to coincide with the normal circadian peak in calcineurin activity[15] and analyzed within the first two hours following isolation.

qPCR. Real-time PCR was performed with SYBR green (Applied Biosystems) as previously described.[8] Data for each transcript was normalized to 18S rRNA as internal control with the 2-ΔΔCt method. Primers used were as follows:

Hk2 rat forward 5'-CGAATCAAAGAGAA CAAGGG-3'
Hk2 rat reverse 5'-CAAAATGGGGATGTTTCTTG-3'
Pfkfb2 rat forward 5'-CTGGAGGTAAAAGTGTCAAG-3'
Pfkfb2 rat reverse 5'-ACGAGAGGTCCTTATCATAG-3'
Slc2a1 rat forward 5'-CAATATGTGGAGCAACTGTG-3'
Slc2a1 rat reverse 5'- AGTAGGTGAAGATGAAGAAGAG-3'
Atp5b rat forward 5'-GGTACAATGCAGGAAAGAATC-3'
Atp5b rat reverse 5'-CACAGTAGTAGCATCCAAATG-3'
Rcan1.1 rat forward, 5'-GACCCGCGCGTGTTC-3'
Rcan1.1 rat reverse 5'-TGTCATATGTTCTGAAGAGGGATTC-3'
Rcan1.4 rat forward, 5'-CCCGTGAAAAAGCAGAATGC-3'
Rcan1.4 rat reverse 5'-TCCTTGTCATATGTTCTGAAGAGGG-3'
Capnl rat forward 5'-TGGAGATCAGTGTCAAGGAGTTAC-3'
Capn1 rat reverse 5'-GCACTCATGCTGCCAGACTTGTCCAGGTCA-3'
Capn2 rat forward 5'-GGGCAGACCAACATCCACCTCAGCAAAAAC-3'
Capn2 rat reverse 5'-ATCTCCGCATCCTCTCCAGCCAGC-3"
POU5F1 human forward 5'-GATCACCCTGGGATATACAC-3'
POU5F1 human reverse 5'-GCTTTGCATATCTCCTGAAG-3'
NANOG human forward 5'-CTATCCATCCTTGCAAATGTC-3'
NANOG human reverse 5'-GTTCTGGTCTTCTGTTTCTTG-3'
SOX2 human forward 5'-ATAATAACAATCATCGGCGG-3'
SOX2 human reverse 5'-AAAAAGAGAGAGGCAAACTG-3'
RCAN1.1 human forward 5'-TCATTGACTGCGAGATGGAG-3'
RCAN1.1 human reverse 5'-TGATGTCCTTGTCATACGTCCT-3'
RCAN1.4 human forward 5'-CTCACTAGGGGCTTGACTGC-3'
RCAN1.4 human reverse 5'-CAGGCAATCAGGGAGCTAAA-3'

Intracellular and mitochondrial Ca^{2+} determinations. For NRVMs, cytosolic Ca^{2+} levels were determined in cardiomyocytes preloaded with Fura2 or Fluo4 (5 μM, 30 min), as described previously.[16] To determine mitochondrial Ca^{2+} levels, images were obtained from cultured cardiomyocytes preloaded with Rhod-FF (5.4 μM, 30 min).[16-18] At the end of each measurement, CCCP 10 μM was used as control.[17] Both determinations were performed in an inverted confocal microscope (Carl Zeiss LSM 5, Pascal 5 Axiovert 200 microscope). For the case of AMVMs, cells were loaded with Rhod2 (10 μM) and treated with Thapsigargin (5 μM) for 20 min. Then, cells were permeabilized with saponin (50 mg/mL) for 1 min in Ca^{2+}-free internal solution (in mM: 5 EGTA, 20 HEPES, 10 NaCl, 100 K^{+}Aspartate, 40 KCl, 1 $MgCl_2$, 2 Maleic acid, 2 Glutamic acid, 5 Pyruvic acid, 0.5 KH_2PO_4, 5 Na_2ATP, 10 GSH, 15 BDM, pH 7.2 Tris). After permeabilization, cells were maintained in Ca^{2+}-free internal solution and then switched to the same internal solution with 2 μM free Ca^{2+} solution (5 mM EGTA and 4.4 mM $CaCl_2$ = 2 μM free Ca^{2+} at pH 7.2, 23ºC, http://maxchelator.stanford.edu/CaMgATPEGTA-TS.htm).[20]

Immunofluorescence Studies and Colocalization Analysis. Cells were fixed, permeabilized, blocked, and incubated with primary antibodies (anti- NFAT, DRP1 and HSPA9). Secondary antibodies were anti-rabbit Alexa 456 for NFAT (A10042), anti-mouse 488 for DRP1 (A21202) and anti-goat 639 for HSPA9 (A21447). ProLong Gold antifade with DAPI was used as mounting medium (Life Technologies, Thermo Fischer Scientific; Waltham, MA, USA). For the colocalization analysis, only one focal plane was analyzed. Images obtained were deconvolved, and background was subtracted with the use of ImageJ software. Colocalization between proteins was quantified by the Mander coefficients[10,19] whereas, for NFAT analysis, total fluorescence was normalized to nuclei area before comparison. To control for unspecific fluorescence signals, sections were incubated with secondary antibody alone and photographed at similar intensities to compare with the signal obtained from their respective primary antibodies (Online Figure XIII).

Statistical analysis. Data shown are mean ± SEM of the number of independent experiments indicated (*n*) and represent experiments performed on at least three separate occasions with similar outcomes. Data were analysed by one-way or two-way ANOVA accordingly, and comparisons between groups were performed using a protected Tukey's test. Statistical significance was defined as $P < 0.05$.

Supplemental References

1. Oh M, Dey A, Gerard RD, Hill JA, Rothermel BA. The CCAAT/enhancer binding protein beta (C/EBPbeta) cooperates with NFAT to control expression of the calcineurin regulatory protein RCAN1-4. *J Biol Chem*. 2010;285:16623–16631.

2. Alghanem AF, Wilkinson EL, Emmett MS, Aljasir MA, Holmes K, Rothermel BA, Simms VA, Heath VL, Cross MJ. RCAN1.4 regulates VEGFR-2 internalisation, cell polarity and migration in human microvascular endothelial cells. *Angiogenesis*. 2017;Aug;20(3):341-358

3. Vega RB, Rothermel BA, Weinheimer CJ, Kovacs A, Naseem RH, Bassel-Duby R, Williams RS, Olson EN. Dual roles of modulatory calcineurin-interacting protein 1 in cardiac hypertrophy. *Proc Natl Acad Sci USA*. 2003;100:669–674.

4. Ni YG, Berenji K, Wang N, Oh M, Sachan N, Dey A, Cheng J, Lu G, Morris DJ, Castrillon DH, Gerard RD, Rothermel BA, Hill JA. Foxo transcription factors blunt cardiac hypertrophy by inhibiting calcineurin signaling. *Circulation*. 2006;114:1159–1168.

5. Parra V, Moraga F, Kuzmicic J, López-Crisosto C, Troncoso R, Torrealba N, Criollo A, Díaz-Elizondo J, Rothermel BA, Quest AFG, Lavandero S. Calcium and mitochondrial metabolism in ceramide-induced cardiomyocyte death. *Biochim Biophys Acta*. 2013;1832:1334–1344.

6. Li, D., Wu, J., Bai, Y., Zhao, X., and Liu, L. Isolation and culture of adult mouse cardiomyocytes for cell signaling and in vitro cardiac hypertrophy. *J Vis Exp*. 2014 May 21;(87)

7. Maclean GA, Menne TF, Guo G, Sanchez DJ, Park I-H, Daley GQ, Orkin SH. Altered hematopoiesis in trisomy 21 as revealed through in vitro differentiation of isogenic human pluripotent cells. *Proceedings of the National Academy of Sciences*. 2012;109:17567–17572.

8. Durkin ME, Qian X, Popescu NC, Lowy DR. Isolation of Mouse Embryo Fibroblasts. *Bio Protoc*. 2013;3.

9. Parra V, Verdejo HE, Iglewski M, del Campo A, Troncoso R, Jones D, Zhu Y, Kuzmicic J, Pennanen C, López-Crisosto C, Jaña F, Ferreira J, Noguera E, Chiong M, Bernlohr DA, Klip A, Hill JA, Rothermel BA, Abel ED, Zorzano A, Lavandero S. Insulin stimulates mitochondrial fusion and function in cardiomyocytes via the Akt-mTOR-NFκB-Opa-1 signaling pathway. *Diabetes*. 2014;63:75–88.

10. Parra V, Eisner V, Chiong M, Criollo A, Moraga F, Garcia A, Härtel S, Jaimovich E, Zorzano A, Hidalgo C, Lavandero S. Changes in mitochondrial dynamics during ceramide-induced cardiomyocyte early apoptosis. *Cardiovasc Res*. 2008;77:387–397.

11. Yu T, Sheu S-S, Robotham JL, Yoon Y. Mitochondrial fission mediates high glucose-induced cell death through elevated production of reactive oxygen species. *Cardiovasc Res*. 2008;79:341–351.

12. Bravo R, Vicencio JM, Parra V, Troncoso R, Munoz JP, Bui M, Quiroga C, Rodriguez AE, Verdejo HE, Ferreira J, Iglewski M, Chiong M, Simmen T, Zorzano A, Hill JA, Rothermel BA, Szabadkai G, Lavandero S. Increased ER-mitochondrial coupling promotes mitochondrial respiration and bioenergetics during early phases of ER stress. *J Cell Sci*. 2011;124:2143–2152.

13. Liu Q, D'Silva P, Walter W, Marszalek J, Craig EA. Regulated Cycling of Mitochondrial Hsp70 at the Protein Import Channel. *Science*. 2003;Apr 4;300(5616):139-41

14. Kuzmicic J, Parra V, Verdejo HE, López-Crisosto C, Chiong M, Garcia L, Jensen MD, Bernlohr DA, Castro PF, Lavandero S. Trimetazidine prevents palmitate-induced mitochondrial fission and dysfunction in cultured cardiomyocytes. *Biochemical Pharmacology*. 2014;91:323–336.

15. Sachan N, Dey A, Rotter D, Grinsfelder DB, Battiprolu PK, Sikder D, Copeland V, Oh M, Bush E, Shelton JM, Bibb JA, Hill JA, Rothermel BA. Sustained hemodynamic stress disrupts normal circadian rhythms in calcineurin-dependent signaling and protein phosphorylation in the heart. *Circ Res*. 2011;108:437–445.

16. Chiong M, Parra V, Eisner V, Ibarra C, Maldonado C, Criollo A, Bravo R, Quiroga C, Contreras A, Vicencio JM, Cea P, Bucarey JL, Molgó J, Jaimovich E, Hidalgo C, Kroemer G, Lavandero S. Parallel activation of Ca(2+)-induced survival and death pathways in cardiomyocytes by sorbitol-induced hyperosmotic stress. *Apoptosis :* 2010;15:887–903.

17. Gutierrez T, Parra V, Troncoso R, Pennanen C, Contreras-Ferrat A, Vasquez-Trincado C, Morales PE, López-Crisosto C, Sotomayor-Flores C, Chiong M, Rothermel BA, Lavandero S. Alteration in

mitochondrial Ca 2+ uptake disrupts insulin signaling in hypertrophic cardiomyocytes. *Cell Commun Signal*. 2014;12:68.

18. Rojas-Rivera D, Díaz-Elizondo J, Parra V, Salas D, Contreras A, Toro B, Chiong M, Olea-Azar C, Lavandero S. Regulatory volume decrease in cardiomyocytes is modulated by calcium influx and reactive oxygen species. *FEBS Lett*. 2009;583:3485–3492.

19. Manders EM, Stap J, Brakenhoff GJ, van Driel R, Aten JA. Dynamics of three-dimensional replication patterns during the S-phase, analysed by double labelling of DNA and confocal microscopy. *J Cell Sci*. 1992;103 (Pt 3):857–862.

20. Lu X, Kwong JQ, Molkentin JD, Bers DM. Individual Cardiac Mitochondia Undergo Rare Transient Permeability Transition Pore Openings. *Circ Res* 2016;118:834-41.

Online Figure Legends

Online Figure I. siRNA-mediated depletion of RCAN1 from NRVM. Cells were transfected with a nonspecific control siRNA or ones targeting *RCAN1.1* and *RCAN1.4*, individually or combined (dKD) as indicated. **(A)** Representative Western blots and quantification by densitometry from 3 separate experiments. β-tubulin (TUBB) was used as a loading control. **(B-F)** An independent set of siRNAs targeting total RCAN1 (both transcripts simultaneously (*Rcan1* rat stealth siRNA, cat# RSS332844, Life technologies) was used to deplete RCAN1 from NRVM. **(B)** Changes in protein levels were assessed by Western blot and quantified by densitometry. **(C)** Mitotracker Green was used to assess the mitochondrial network and quantify changes in **(D)** the number and **(E)** size of mitochondria. **(F)** O_2 consumption was compared in NRVMs depleted of total RCAN1 with those depleted of RCAN1.1 alone. Values are mean ± SEM; **P*<0.05, ***P*<0.01, ****P*<0.001.

Online Figure II. Mitochondrial fission is increased in RCAN1.1-depleted NRVM. Cells were transfected with siRNAs as indicated and analyzed 48 h later. **(A)** Electron micrographs of siRNA treated NRVMs (Scale bars = 2 μm and 1 μm). Mitochondrial morphology was quantified for **(B)** cross-sectional area of individual mitochondria, **(C)** mitochondrial density, **(D)** perimeter, and **(E)** circularity index. Data are from 100 mitochondria in each group from three separate experiments. **(F-G)** Western blot analysis of total protein extracts from siRNA depleted NRVM shows a decrease in OPA1 protein levels (long and short isoforms) when RCAN1.1 is depleted, but no change in total DRP1, HSPA9 (also known as mtHSP70), or MFN2. Quantification is from 4 separate experiments. Protein content was normalized to TUBB or GAPDH as indicated. **(H)** Analysis of Mitotracker Green-loaded cells by flow cytometry indicated no change in total mitochondrial content. Values are mean ± SEM; **P*<0.05, ***P*<0.01, ****P*<0.001.

Online Figure III. Either FK506 or Mdivi-1 restore the mitochondrial network to RCAN1.1 depleted NRVM. Cells were transfected with a nonspecific control siRNA or ones targeting *RCAN1.1* as indicated. Following transfection cultures were treated with vehicle, 20 nM FK506, or 12.5 μM Mdivi-1, then analyzed 48 h later. **(A)** Representative images of cardiomyocytes stained with Mitotracker Green shows treatment with FK506 increases mitochondrial fusion in the RCAN1.1-depleted cells (Scale bar: 20 mm). This is quantified in **(B-C)**. Panels **(D-F)** present similar analysis for Mdivi-1treatment. Data are from 20 cells examined from four separate experiments (*N=4*). (**G**) Representative confocal images of immunocytochemistry for NFAT (red), DRP1 (green), mitochondrial HSPA9 (magenta) and nucleus (blue) in siRNA transfected NRVM. Lower panels provide magnified image of marked region of interest. Scale bar: 20 μm. (**H**) Relative levels of nuclear NFAT fluorescence, quantified from images in A. (**I**) Mander's coefficient quantification of DRP1 colocalization with the mitochondrial marker HSPA9. (**J**) Number of mitochondria per cell and (**K**) mitochondrial area assessed using HSPA9 signal in the images in A (*n=25 cells x 4 experiments*). Values are mean ± SEM; **P*<0.05, ***P*<0.01, ****P*<0.001.

Online Figure IV. RCAN1.1-depleted NRVMs show increased dependence on glycolysis and sensitivity to I/R that is normalized by treatment with FK506 or Mdivi-1. NRVM were transfected with siRNAs and treated as indicated then analyzed 48 h later. **(A)** NRVM were loaded with TMRM and analyzed by flow cytometry to assess $\Delta\psi_m$. In the presence or absence of the complex V inhibitor, Oligomycin (Oligo, 10 μM) (*n=5*). (**B**) LDH release was measured in media with and without glucose (*n=4*). **(C-H)** Transcript levels for *Hk2,* P*fkfb2* and, *Slc2a1*were elevated in the RCAN1.1-depleted and dKD cells. Incubation with either 20 nM FK506 or 12.5 μM Mdivi-1 reduced transcript levels to those found in control cells. (**I-J**) Western blot analysis of total protein from NRVM before and after sI/R (I/R) showed no change in the levels of RCAN1 and RCAN1.4. Quantification below is from 4 separate experiments *(n=4)*. Protein loading was normalized to GAPDH. **(K-L)** Either FK506 or Mdivi-1

conferred significant protection from simulated I/R to NRVM depleted of RCAN1 (dKD). (*n=5*). Values are mean ± SEM; **P*<0.05, ***P*<0.01, ****P*<0.001.

Online Figure V. Radial profile analysis of mitochondrial distribution in RCAN1 depleted NRVM. **(A)** Schematic of subcellular zones applied for fluorescence analysis. **(B)** Quantification of mitochondrial volume in each of the radial zones, applied to control or RCAN1.1 depleted NRVM. Data are from 25 cells examined from six separate experiments (*n=6*). Mean ± SEM; **P*<0.05 compared with si*Control*.

Online Figure VI. RCAN1-depleted NRVM are more sensitive to CAPN-mediated damage following I/R. **(A)** Cytosolic Ca^{+2} was assessed by loading cells with Fluo4 prior to the addition of Histamine (100 μM) to release Ca^{+2} from ER stores. (**B**) Signal from A was quantified as the maximal fluorescence ratio reached during the first 150 s. Data are from 40 cells examined in five separate experiments *(n=4)*. (**C**) α-spectrin cleavage products were assessed by Western blot as an indication of calpain activity in RCAN1.1-depleted NRVMs pretreated with Mdivi (12.5 μM) or vehicle. (**D**) Densitometry quantification of data from C *(n=4)*. **(E-G)** NRVM were transfected with control siRNA or ones targeting both RCAN1.1 and RCAN1.4 (dKD) as indicated**.** 48 h following transfection three different calpain inhibitors were tested for their ability to restore protection from simulated I/R: **(E)** 10 μM E-64D, **(F)** 10 μM MDL, or **(G)** 10 μM PD 150606. All three conferred protection to the dKD cells (*n=5*). **(H)** A mixture of siRNA's targeting Calpain (*Capn*) 1 and 2 (50 nM) also conferred protection to the RCAN dKD NRVMs (*n=5*). **(I-J)** Transcript levels for *Capn1* and *Capn2* were quantified by qPCR in NRVMs treated with the mixture of siRNA's depleting *Capn 1* and *2* (*n=3*). (**K**) LDH release in RCAN1.1-depleted NRVMs subjected to sI/R and preincubated with either RuRed (10 μM) or BAPTA AM (1 μM) prior ischemia (*n=4*). (**L-O**) Validation of RuRed and BAPTA AM to alter Ca^{+2} handing (MCU inhibition and chelation of cytoplasmic Ca^{2+} respectively). In L-M cells where loaded with Rhod-FF, whereas in N-O cells where loaded with Fluo4. Data are from 40 cells examined in four separate experiments *(n=4)*. Values are mean ± SEM; **P*<0.05, ***P*<0.01, ****P*<0.00.

Online Figure VII. Adenoviral expression of human *RCAN1.1*. NRVM were transduced with an adenovirus encoding HA-tagged human RCAN1.1 (*Ad-RCAN1.1*) or β-galactosidase (*Ad-β-gal*) as a control (MOI 0-1,000). 48 h later, cells where assayed for **(A)** LDH release as control for toxicity (*n=4*); **(B)** Transcript and *RCAN1,1* and **(C-D)** protein levels of hRCAN1.1 (*n=3*). Values are mean ± SEM; **P*<0.05, ****P*<0.001.

Online Figure VIII. Adenoviral expression of human *RCAN1.4*. NRVM were transduced with an adenovirus encoding human RCAN1.4 (*Ad-RCAN1.4*) or β-galactosidase (*Ad-β-gal*) as a control (MOI 0-1,000). 48 h later, cells where assayed for **(A)** LDH release as control for toxicity (*n=4*). Total cellular extracts were used for the analysis of **(B)** transcript (*n=3*) and **(C-D)** protein levels of RCAN1.4 (*n=3*). **(E)** NRVM were transfected with *Control* and *Rcan1.1*-targeted siRNAs followed by infection with *Ad-RCAN1.4* or *Ad-β-gal* (MOI 100 or 500). 48 h later, cells where loaded with Mitotracker Green and imaged by confocal (*n=4*). Scale bar = 10 μm. **(F)** The number of mitochondria per cell and **(G)** individual mitochondrial volume were quantified. **(H)** Infection with *Ad-RCAN1.4* was not sufficient to restore protection from I/R to siRCAN1.1-depleted NRVMs as assayed by LDH release (*n=4*). Values are mean ± SEM; **P*<0.05, ***P*<0.01, ****P*<0.001.

Online Figure IX. Validation of mitochondrial Ca^{2+} uptake. **(A)** Representative images of Rhod2 signal following switch to 2 μM free Ca^{2+} solution in AMVM isolated from *WT* animals. Higher magnification shows pattern of staining foci consistent with mitochondrial morphology, as opposed to a cytosolic pattern. **(B)** The addition of 2 μM RuRed inhibited increase in mitochondrial Ca^{2+} signal, validating uptake via MCU**.** Scale Bar = 8 μm.

Online Figure X. MEF from *Rcan1 KO* mice show evidence of increased mitochondrial fragmentation. (A) Representative confocal Z-stack reconstructions of MEFs derived from *WT* and *Rcan1 KO* embryos stained with Mitotracker Green show increased mitochondrial fragmentation in *KO* cells compared to *WT* (Scale bar = 20 μm). **(B)** Number of mitochondria per cell and **(C)** individual mitochondrial volume were quantified. Data are from 15 cells examined from three separate experiments (*n=3*). Values are mean ± SEM; ***P*<0.01.

Online Figure XI. siRNA depletion of RCAN1.1 from disomic (2S) and trisomic (3S) iPSC did not affect expression of genes indicative of pluripotency. siRNA-depleted iPSC were analyzed by qPCR for POU class 5 homeobox (POU5F1, also known as OCT3/4), Nanog homeobox (NANOG) and SRY-box 2 (SOX2) expression. HEK293 cells were used as controls for the absence of these markers (*n=4*). Values represent the mean ± SEM.

Online Figure XII. Schematic model depicting RCAN1's role in maintaining a metabolically active mitochondrial network. When RCAN1 levels are low, calcineurin (CN) is more easily activated, increasing the potential for translocation of DRP1 to mitochondria to promote fission. The resulting mitochondrial population has a lower membrane potential with decreased O_2 consumption, ROS generation, and capacity for mitochondrial Ca^{2+} uptake. As a consequence cytosolic Ca^{2+} remains elevated longer following I/R increasing CAPN-mediated damage. Increased RCAN1 levels helps preserve fusion and reduce I/R activation of CAPN.

Online Figure XIII. IgG controls for DRP1, NFAT and HSPA9 immunofluorescences. Representative confocal images of immunocytochemistry for DRP1 (green), NFAT (red), mitochondrial HSPA9 (magenta) and their respective controls of IgG-alexa conjugated secondary antibodies in NRVM. Scale bar: 20 μm.

Online Table I: Antibody source and validation

Antibody	Catalog Number	source	Host	Immmunoglobin Fragment	dilution	Validation
Anti-OPA1	ab42364	Abcam	Rabbit Polyclonal	aa 900 to the C-terminus of Rat OPA1	1:1000 (WB)	Adenovirus Opa1 PMID: 24009260
Anti-MFN2	ab50838	Abcam	Rabbit Polyclonal	peptide: KINGIFEQLGA YIQESAT corresponding to N terminal aa 38-55 of Human MFN2	1:1000 (WB)	Adenovirus, Antisense Mfn2 PMID: 24009260, 27808250
Anti-PINK1	ab23707	Abcam	Rabbit Polyclonal	peptide: LVRALLQREA SKRPSARVAAN corresponding to aa 484-504 of Human PINK1.	1:1000 (WB)	Signal following CCCP treatment Molecular Weight. PMID: 24897381
Anti-VDAC	ab14734	Abcam	Mouse Monoclonal	full length Human VDAC	1:1000 (WB)	Mitochondrial marker (loading control) used extensively in the literature.
Anti-SOX2	ab97959	Abcam	Rabbit Polyclonal	aa 300 to the C-terminus of Human SOX2.	1:500 (WB)	Pluripotency marker used extensively Stanford University Human Pluripotency Stem Cell Laboratory Manual 2015
Anti-PHOSPHO-DRP1	4867	Cell Signaling	Rabbit Polyclonal	phosphopeptide surrounding Ser637 of Human DRP1	1:500 (WB)	20 mM of Forskolin stimulation (30 min), Molecular Weight. PMID: 24777478, 26807480
Anti-GAPDH	2118	Cell Signaling	Rabbit Polyclonal	carboxy terminus of Human GAPDH.	1:2000 (WB)	Cytosolic marker and loading control extensively used in the literature.
Anti-NFAT1	5861	Cell Signaling	Rabbit Polyclonal	synthetic peptide corresponding to residues surrounding Gly87 of Human NFAT1	1:100 (IF)	10 mM of NE stimulation (24 h). PMID: 27977752 Nuclear translocation following RCAN1 siRNA
Anti-PARK2	MAB5512	Merck Millipore	Mouse Monoclonal	Full lentgh Human PARKIN	1:500	Molecular Weight following CCCP PMID: 24897381
Anti-α-SPTAN1	MAB1622	Merck Millipore	Mouse Monoclonal	Chicken red blood cell membranes	1:1000 (WB)	CAPN induction and siRNA against CAPN, PMID: 20026269, 23602992
Anti-HSPA9	MA3-028	Thermo Fischer Scientific	Mouse Monoclonal	Peptide: GSGSSGTGEQKEDQKE EKQ corresponding to aa 615-633 of Mouse mtHSP70.	1:1500 (WB) 1:500 (IF)	Mitochondrial marker (loading control) used extensively in the literature. PMID: 18006463, 24009260, 27808250
Anti-HSPA9	PA5-48035	Thermo Fischer	Goat Polyclonal	E. coli-derived recombinant Human GRP75 aa 542-679	1:100 (IF)	IF colocalization with MA3-028.

Anti-DRP1	611112	Becton-Dickinson	Mouse Monoclonal	Rat DLP1 aa 601-722	1:500 (WB) 1:100 (IP)	Adenovirus DRP1 WT and DN K38A. PMID: 24777478, 28739174 Mitochondrial colocalization following siRCAN1
Anti-POU5F1	SC-5279	Santa Cruz	Mouse Monoclonal	aa 1-134 of Human Oct-3/4	1:500 (WB)	Pluripotency marker used extensively Stanford University Human Pluripotency Stem Cell Laboratory Manual 2015
Anti-TUBB	T4026	Sigma-Aldrich	Mouse Monoclonal	Purified rat brain tubulin.	1:5000 (WB)	Cytosolic marker and loading control used extensively in the literature.
Anti-RCAN1	D6694	Sigma-Aldrich	Rabbit Polyclonal	aa 235-252 of Human DSCR1,	1:2000 (WB)	Over expression and siRNA against RCAN1 isoforms 1.1 and 1.4. 10 mM of NE stimulation (24 h). PMID: 24838101, 24777478

ONLINE FIGURE I

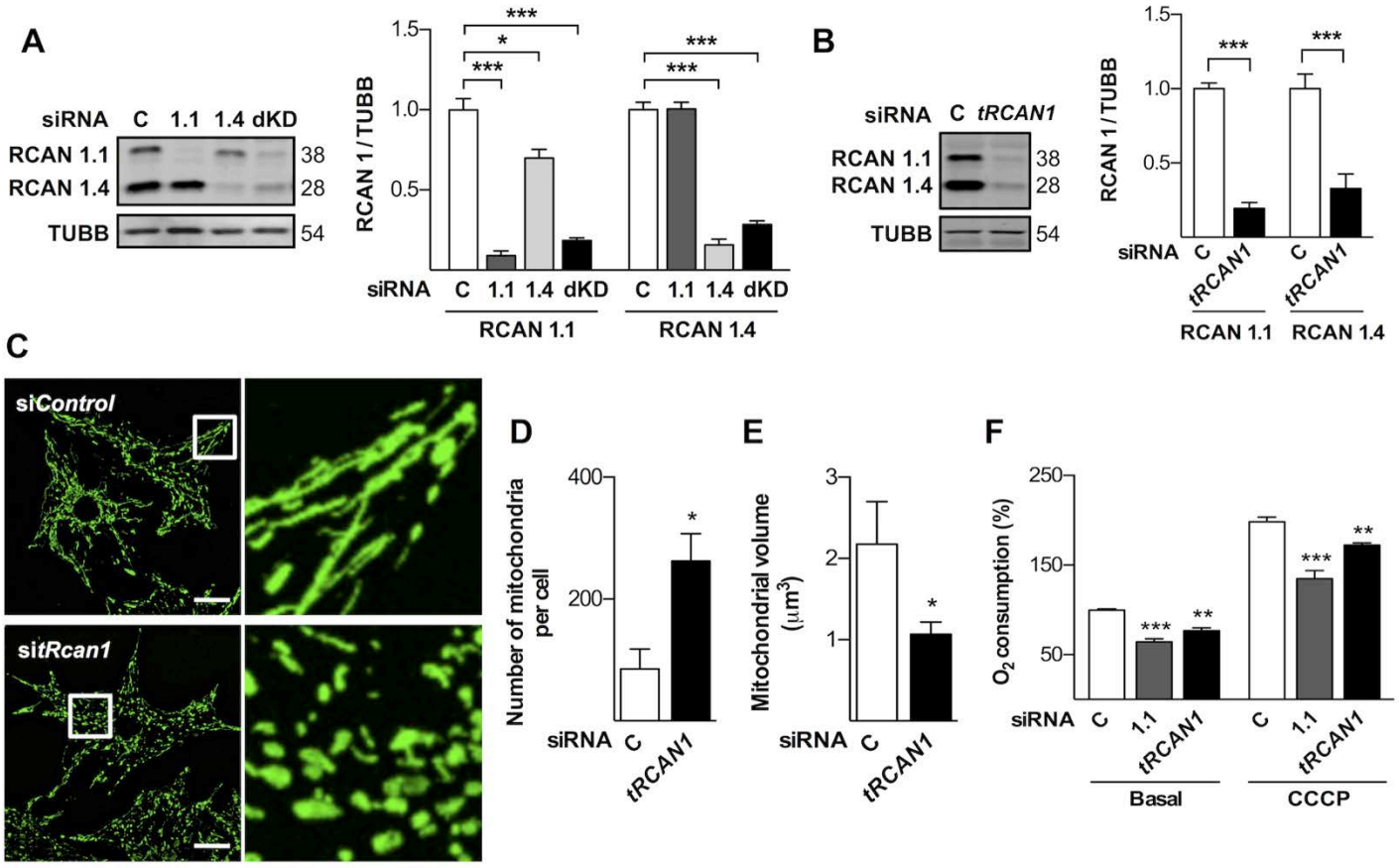

Online Figure I. siRNA-mediated depletion of RCAN1 from NRVM. Cells were transfected with a nonspecific control siRNA or ones targeting *RCAN1.1* and *RCAN1.4*, individually or combined (dKD) as indicated. **(A)** Representative Western blots and quantification by densitometry from 3 separate experiments. β-tubulin (TUBB) was used as a loading control. **(B-F)** An independent set of siRNAs targeting total RCAN1 (both transcripts simultaneously (*Rcan1* rat stealth siRNA, cat# RSS332844, Life technologies) was used to deplete RCAN1 from NRVM. **(B)** Changes in protein levels were assessed by Western blot and quantified by densitometry. **(C)** Mitotracker Green was used to assess the mitochondrial network and quantify changes in **(D)** the number and **(E)** size of mitochondria. **(F)** O_2 consumption was compared in NRVMs depleted of total RCAN1 with those depleted of RCAN1.1 alone. Values are mean ± SEM; **P*<0.05, ***P*<0.01, ****P*<0.001.

ONLINE FIGURE II

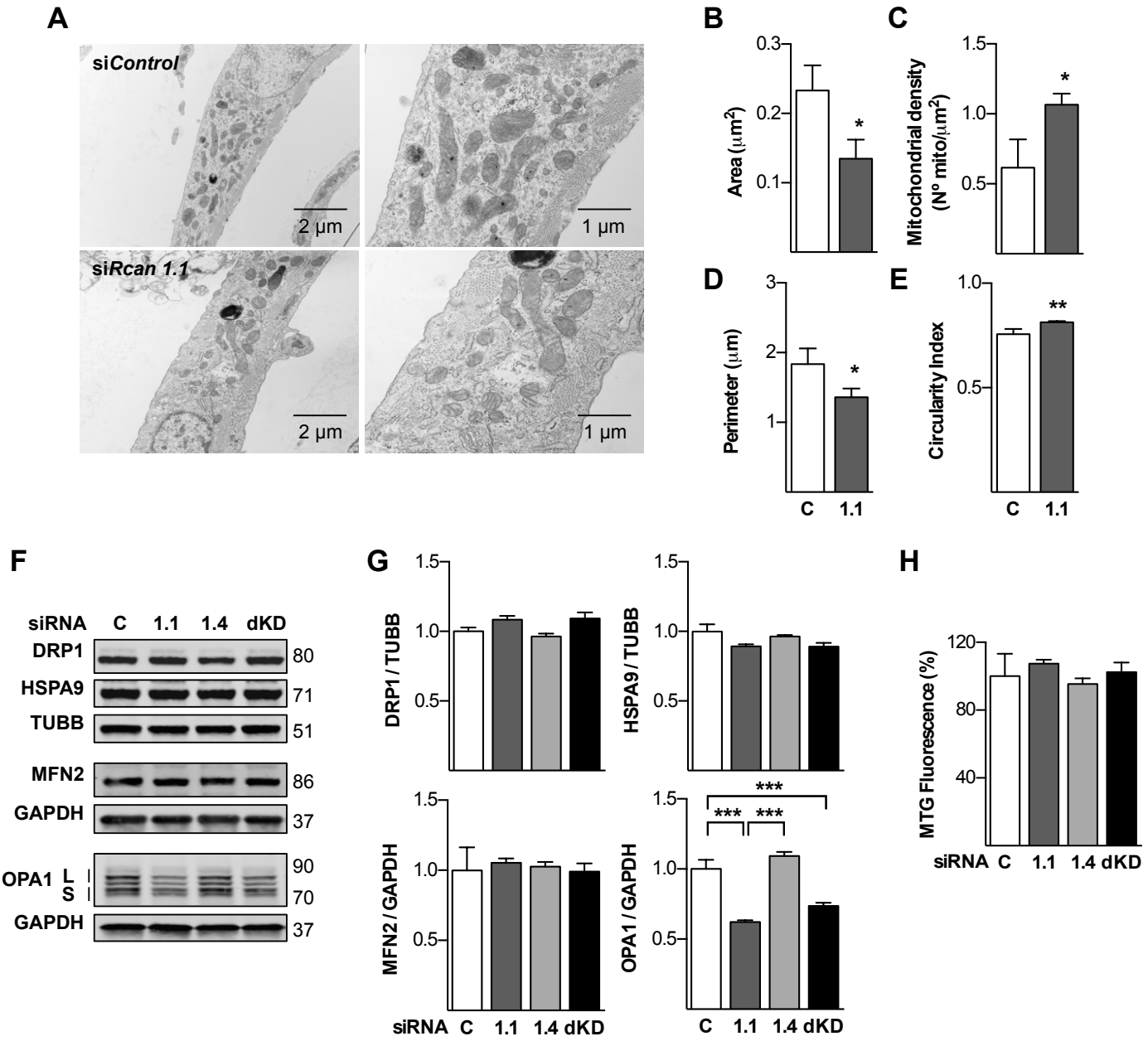

Online Figure II. Mitochondrial fission is increased in RCAN1.1-depleted NRVM. Cells were transfected with siRNAs as indicated and analyzed 48 h later. **(A)** Electron micrographs of siRNA treated NRVMs (Scale bars = 2 µm and 1 µm). Mitochondrial morphology was quantified for **(B)** cross-sectional area of individual mitochondria, **(C)** mitochondrial density, **(D)** perimeter, and **(E)** circularity index. Data are from 100 mitochondria in each group from three separate experiments. **(F-G)** Western blot analysis of total protein extracts from siRNA depleted NRVM shows a decrease in OPA1 protein levels (long and short isoforms) when RCAN1.1 is depleted, but no change in total DRP1, HSPA9 (also known as mtHSP70), or MFN2. Quantification is from 4 separate experiments. Protein content was normalized to TUBB or GAPDH as indicated. **(H)** Analysis of Mitotracker Green-loaded cells by flow cytometry indicated no change in total mitochondrial content. Values are mean ± SEM; **P*<0.05, ***P*<0.01, ****P*<0.001.

ONLINE FIGURE III

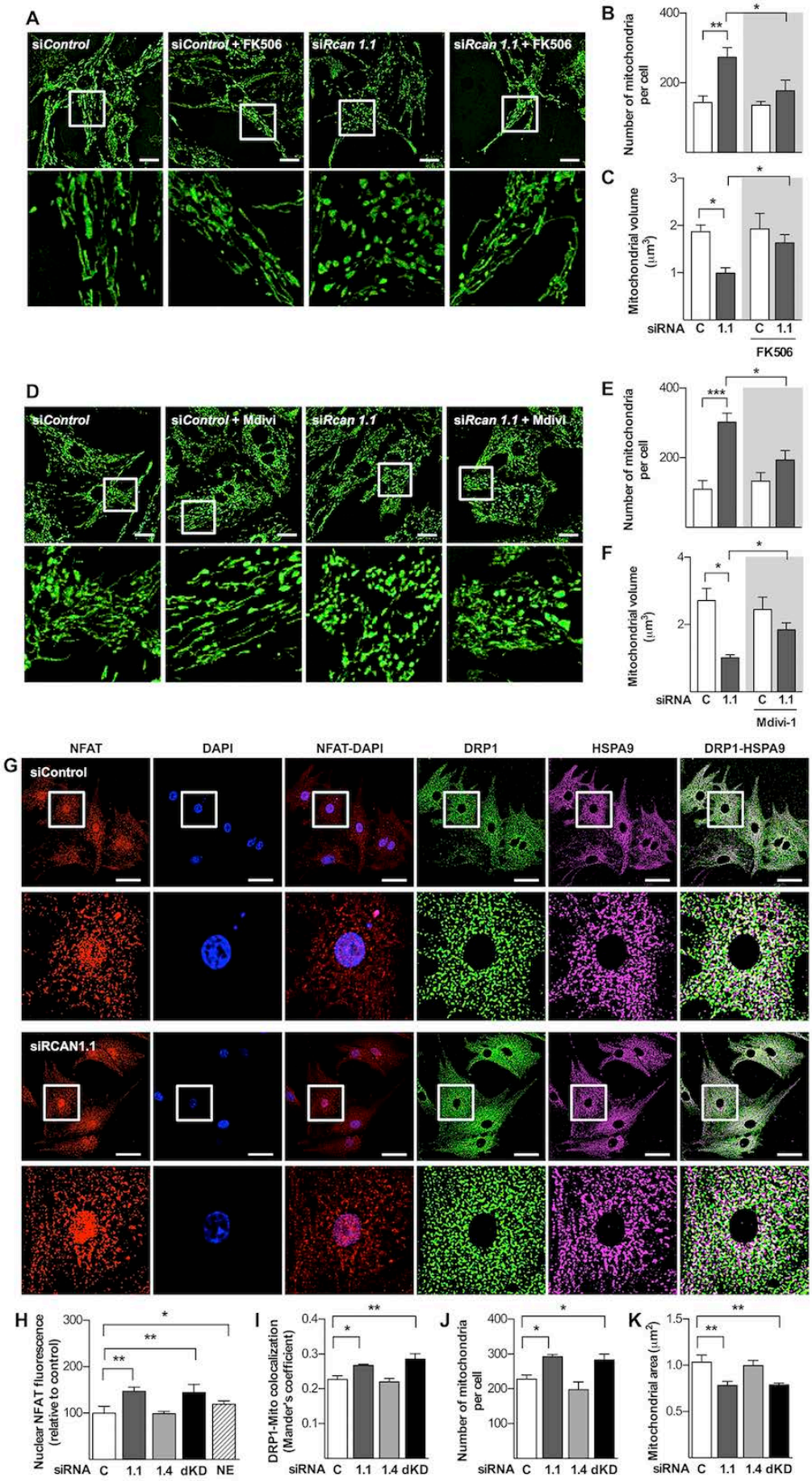

Online Figure III. Either FK506 or Mdivi-1 restore the mitochondrial network to RCAN1.1 depleted NRVM. Cells were transfected with a nonspecific control siRNA or ones targeting *RCAN1.1* as indicated. Following transfection cultures were treated with vehicle, 20 nM FK506, or 12.5 μM Mdivi-1, then analyzed 48 h later. **(A)** Representative images of cardiomyocytes stained with Mitotracker Green shows treatment with FK506 increases mitochondrial fusion in the RCAN1.1-depleted cells (Scale bar: 20 mm). This is quantified in **(B-C)**. Panels **(D-F)** present similar analysis for Mdivi-1treatment. Data are from 20 cells examined from four separate experiments (*N=4*). (**G**) Representative confocal images of immunocytochemistry for NFAT (red), DRP1 (green), mitochondrial HSPA9 (magenta) and nucleus (blue) in siRNA transfected NRVM. Lower panels provide magnified image of marked region of interest. Scale bar: 20 μm. (**H**) Relative levels of nuclear NFAT fluorescence, quantified from images in A. (**I**) Mander's coefficient quantification of DRP1 colocalization with the mitochondrial marker HSPA9. (**J**) Number of mitochondria per cell and (**K**) mitochondrial area assessed using HSPA9 signal in the images in A (*n=25 cells x 4 experiments*). Values are mean ± SEM; **P*<0.05, ***P*<0.01, ****P*<0.001.

ONLINE FIGURE IV

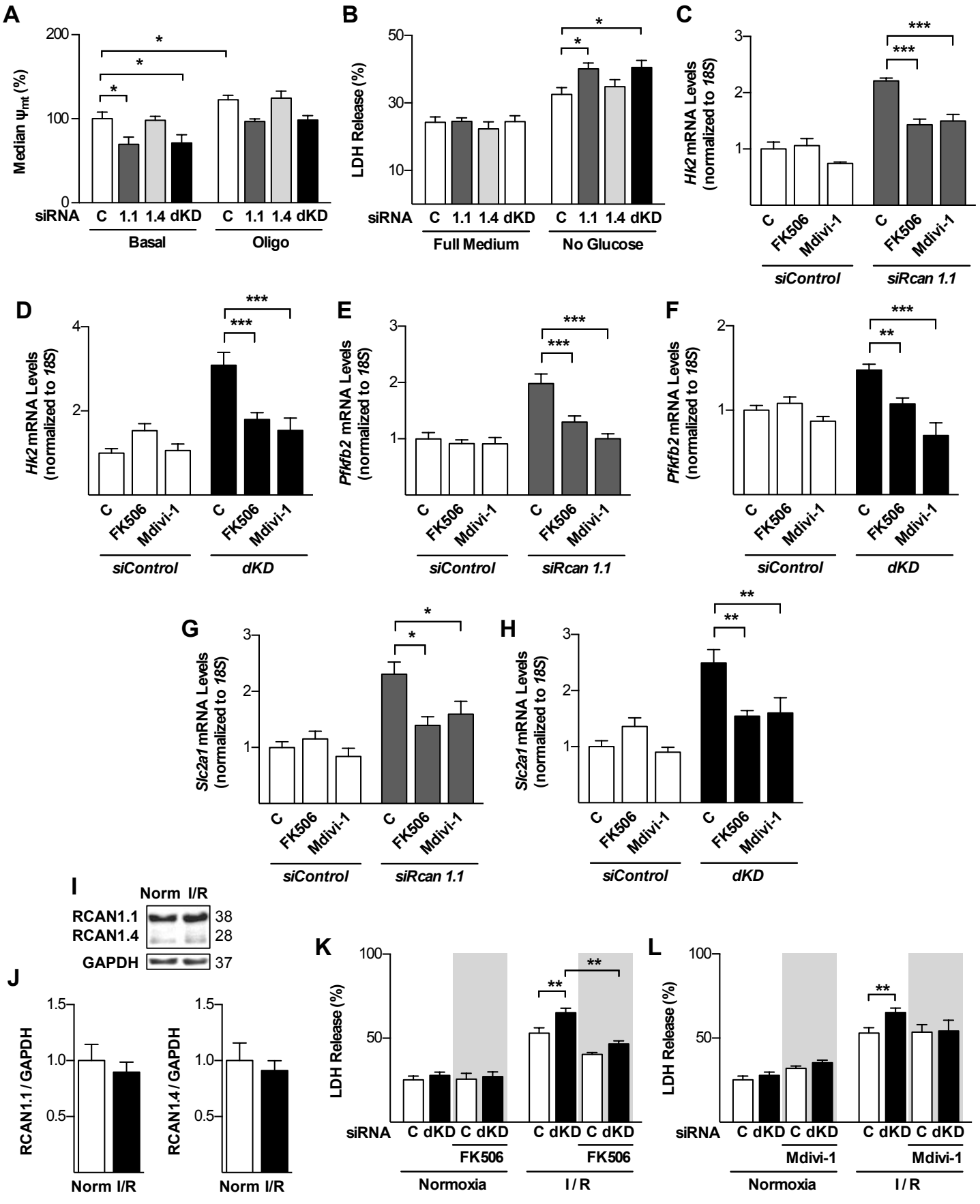

Online Figure IV. RCAN1.1-depleted NRVMs show increased dependence on glycolysis and sensitivity to I/R that is normalized by treatment with FK506 or Mdivi-1. NRVM were transfected with siRNAs and treated as indicated then analyzed 48 h later. **(A)** NRVM were loaded with TMRM and analyzed by flow cytometry to assess $\Delta\psi_m$. In the presence or absence of the complex V inhibitor, Oligomycin (Oligo, 10 μM) (*n=5*). (**B**) LDH release was measured in media with and without glucose (*n=4*). **(C-H)** Transcript levels for *Hk2,* P*fkfb2* and, *Slc2a1*were elevated in the RCAN1.1-depleted and dKD cells. Incubation with either 20 nM FK506 or 12.5 μM Mdivi-1 reduced transcript levels to those found in control cells. (**I-J**) Western blot analysis of total protein from NRVM before and after sI/R (I/R) showed no change in the levels of RCAN1 and RCAN1.4. Quantification below is from 4 separate experiments *(n=4)*. Protein loading was normalized to GAPDH. **(K-L)** Either FK506 or Mdivi-1 conferred significant protection from simulated I/R to NRVM depleted of RCAN1 (dKD). (*n=5*). Values are mean ± SEM; **P*<0.05, ***P*<0.01, ****P*<0.001.

ONLINE FIGURE V

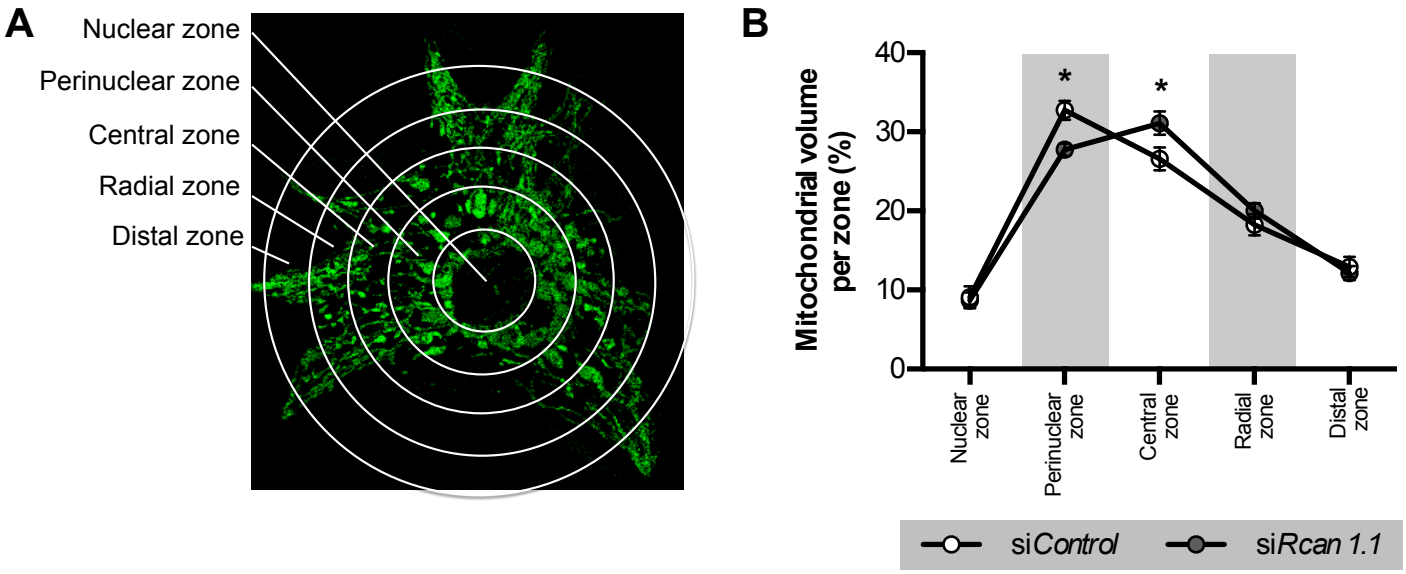

Online Figure V. Radial profile analysis of mitochondrial distribution in RCAN1 depleted NRVM. (A) Schematic of subcellular zones applied for fluorescence analysis. **(B)** Quantification of mitochondrial volume in each of the radial zones, applied to control or RCAN1.1 depleted NRVM. Data are from 25 cells examined from six separate experiments (*n=6*). Mean ± SEM; **P*<0.05 compared with si*Control*.

ONLINE FIGURE VI

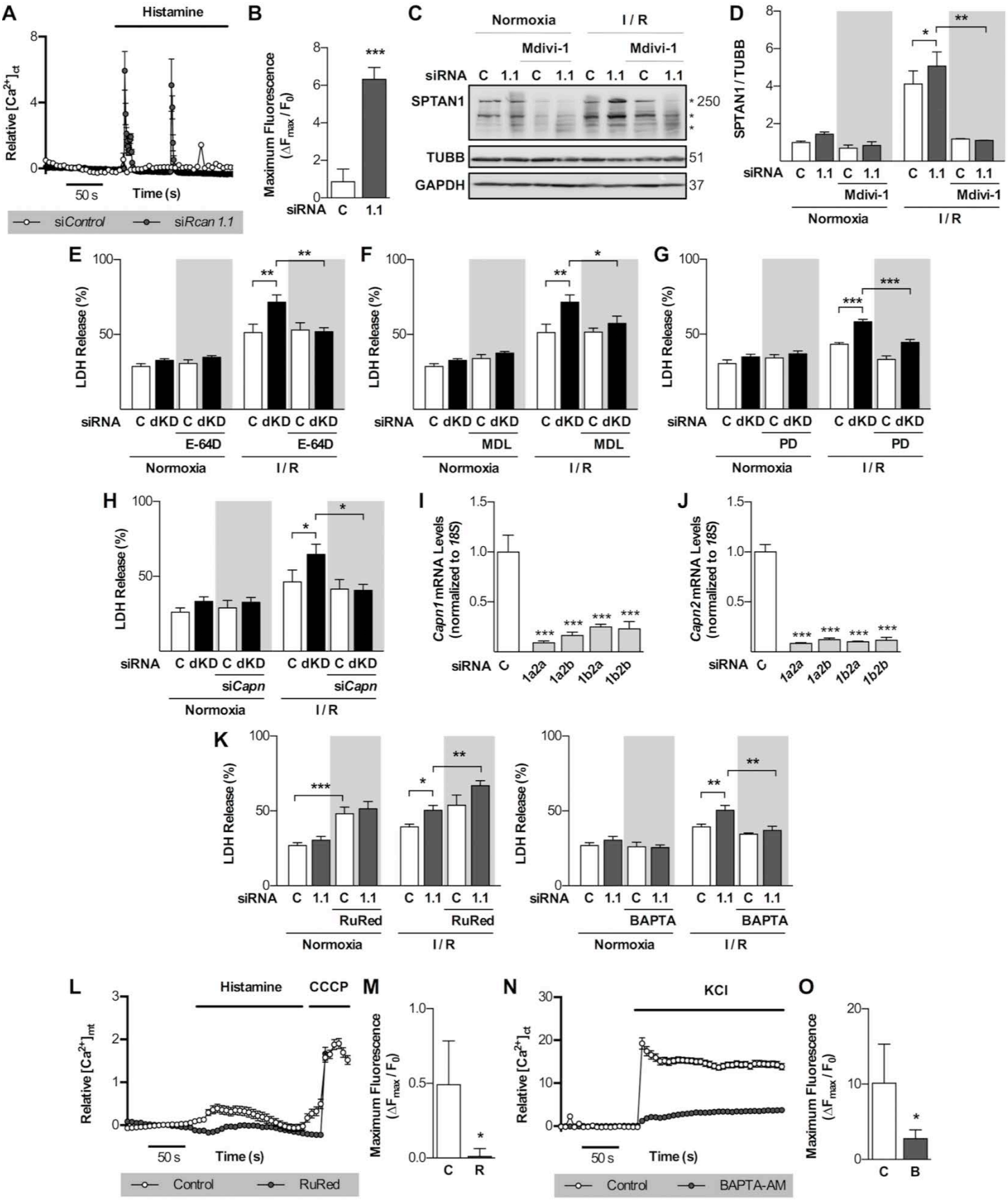

Online Figure VI. RCAN1-depleted NRVM are more sensitive to CAPN-mediated damage following I/R. (A) Cytosolic Ca^{+2} was assessed by loading cells with Fluo4 prior to the addition of Histamine (100 μM) to release Ca^{+2} from ER stores. (**B**) Signal from A was quantified as the maximal fluorescence ratio reached during the first 150 s. Data are from 40 cells examined in five separate experiments *(n=4)*. (**C**) α-spectrin cleavage products were assessed by Western blot as an indication of calpain activity in RCAN1.1-depleted NRVMs pretreated with Mdivi (12.5 μM) or vehicle. (**D**) Densitometry quantification of data from C *(n=4)*. **(E-G)** NRVM were transfected with control siRNA or ones targeting both RCAN1.1 and RCAN1.4 (dKD) as indicated**.** 48 h following transfection three different calpain inhibitors were tested for their ability to restore protection from simulated I/R: **(E)** 10 μM E-64D, **(F)** 10 μM MDL, or **(G)** 10 μM PD 150606. All three conferred protection to the dKD cells (*n=5*). **(H)** A mixture of siRNA's targeting Calpain (*Capn*) 1 and 2 (50 nM) also conferred protection to the RCAN dKD NRVMs (*n=5*). **(I-J)** Transcript levels for *Capn1* and *Capn2* were quantified by qPCR in NRVMs treated with the mixture of siRNA's depleting *Capn 1* and *2* (*n=3*). (**K**) LDH release in RCAN1.1-depleted NRVMs subjected to sI/R and preincubated with either RuRed (10 μM) or BAPTA AM (1 μM) prior ischemia (*n=4*). (**L-O**) Validation of RuRed and BAPTA AM to alter Ca^{+2} handing (MCU inhibition and chelation of cytoplasmic Ca^{2+} respectively). In L-M cells where loaded with Rhod-FF, whereas in N-O cells where loaded with Fluo4. Data are from 40 cells examined in four separate experiments *(n=4)*. Values are mean ± SEM; **P*<0.05, ***P*<0.01, ****P*<0.00.

ONLINE FIGURE VII

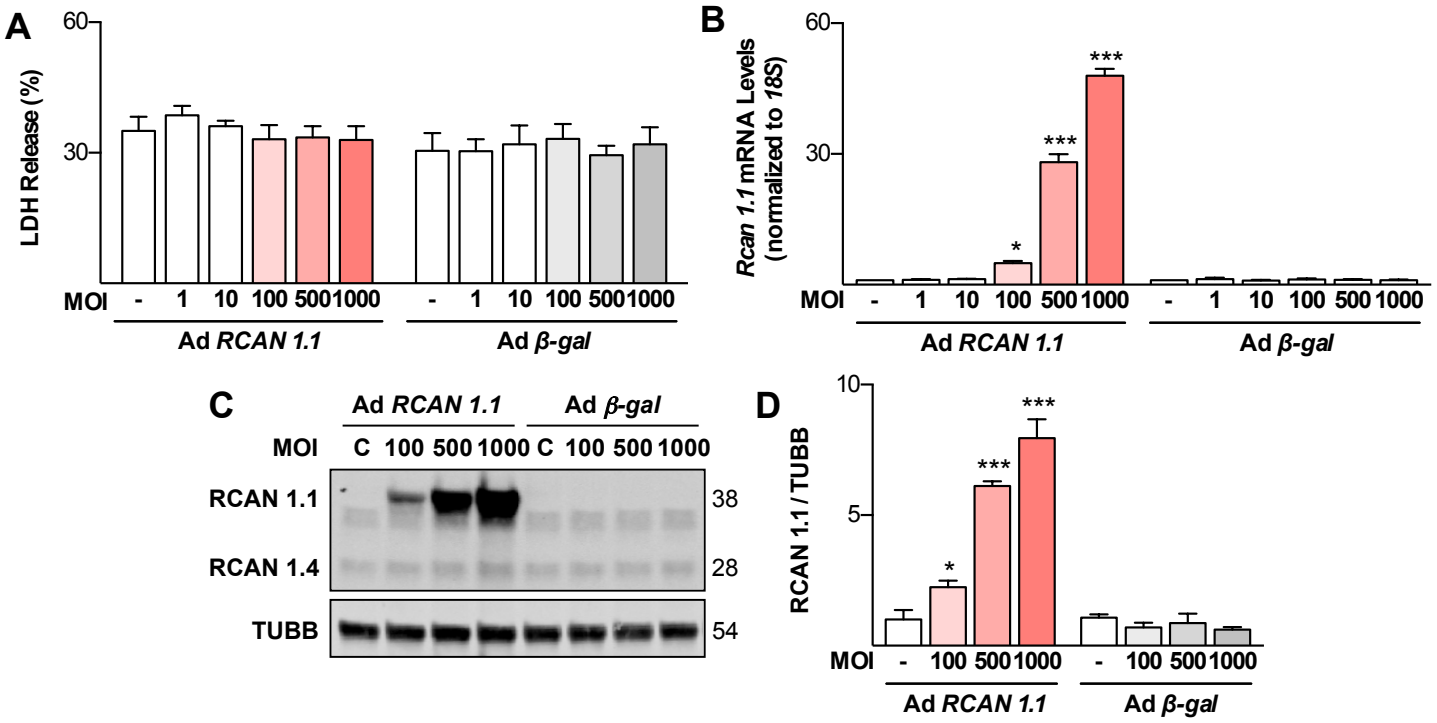

Online Figure VII. Adenoviral expression of human *RCAN1.1*. NRVM were transduced with an adenovirus encoding HA-tagged human RCAN1.1 (*Ad-RCAN1.1*) or β-galactosidase (*Ad-β-gal*) as a control (MOI 0-1,000). 48 h later, cells where assayed for **(A)** LDH release as control for toxicity (*n=4*); **(B)** Transcript and *RCAN1,1* and **(C-D)** protein levels of hRCAN1.1 (*n=3*). Values are mean ± SEM; **P*<0.05, ****P*<0.001.

ONLINE FIGURE VIII

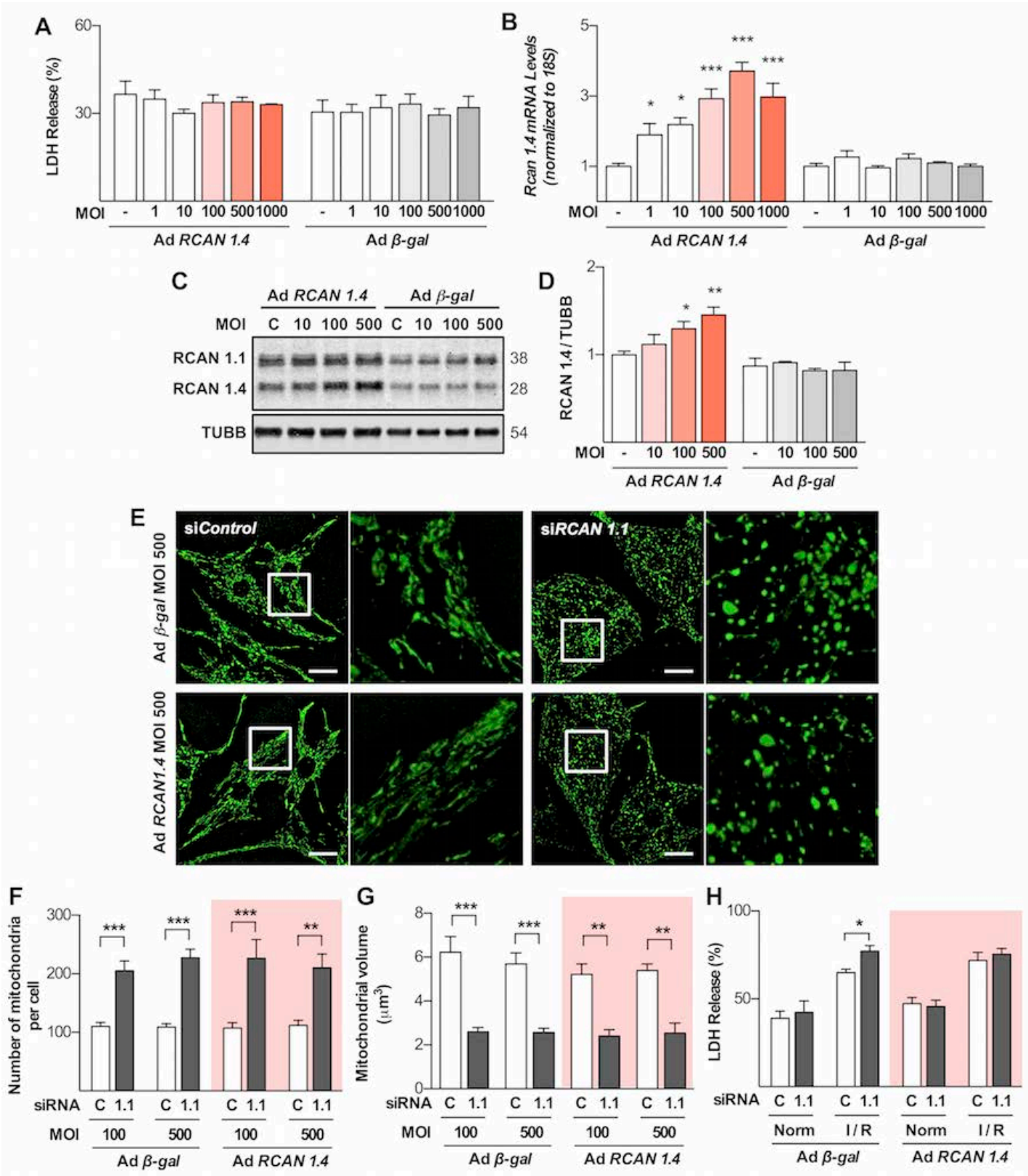

Online Figure VIII. Adenoviral expression of human *RCAN1.4*. NRVM were transduced with an adenovirus encoding human RCAN1.4 (*Ad-RCAN1.4*) or β-galactosidase (*Ad-β-gal*) as a control (MOI 0-1,000). 48 h later, cells where assayed for **(A)** LDH release as control for toxicity (*n=4*). Total cellular extracts were used for the analysis of **(B)** transcript (*n=3*) and **(C-D)** protein levels of RCAN1.4 (*n=3*). **(E)** NRVM were transfected with *Control* and *Rcan1.1*-targeted siRNAs followed by infection with *Ad-RCAN1.4* or *Ad-β-gal* (MOI 100 or 500). 48 h later, cells where loaded with Mitotracker Green and imaged by confocal (*n=4*). Scale bar = 10 μm. **(F)** The number of mitochondria per cell and **(G)** individual mitochondrial volume were quantified. **(H)** Infection with *Ad-RCAN1.4* was not sufficient to restore protection from I/R to siRCAN1.1-depleted NRVMs as assayed by LDH release (*n=4*). Values are mean ± SEM; $*P<0.05$, $**P<0.01$, $***P<0.001$.

ONLINE FIGURE IX

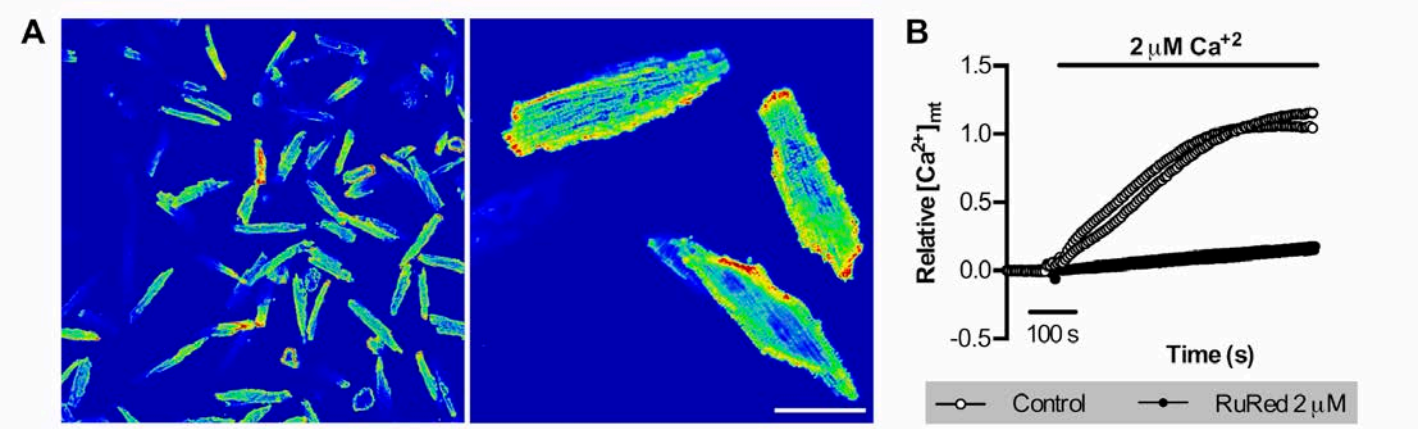

Online Figure IX. Validation of mitochondrial Ca^{2+} uptake. **(A)** Representative images of Rhod2 signal following switch to 2 μM free Ca^{2+} solution in AMVM isolated from *WT* animals. Higher magnification shows pattern of staining foci consistent with mitochondrial morphology, as opposed to a cytosolic pattern. **(B)** The addition of 2 μM RuRed inhibited increase in mitochondrial Ca^{2+} signal, validating uptake via MCU**.** Scale Bar = 8 μm.

ONLINE FIGURE X

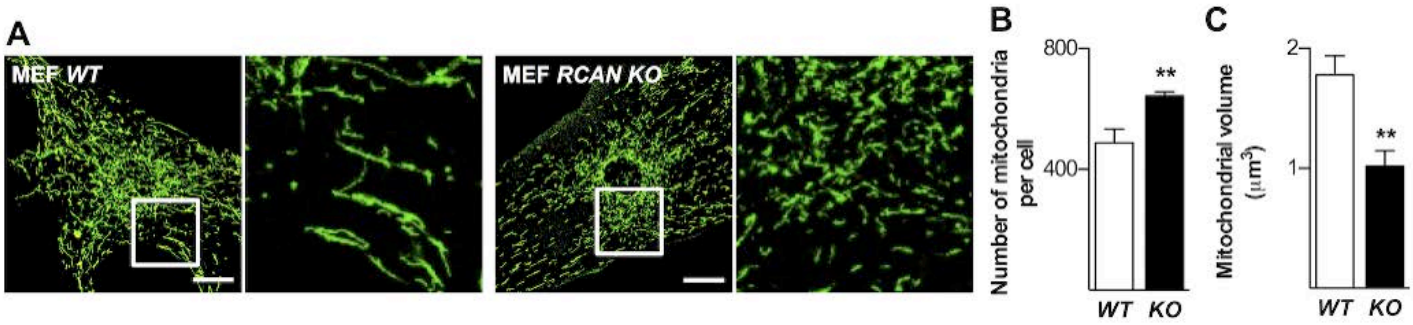

Online Figure X. MEF from *Rcan1 KO* mice show evidence of increased mitochondrial fragmentation. (A) Representative confocal Z-stack reconstructions of MEFs derived from *WT* and *Rcan1 KO* embryos stained with Mitotracker Green show increased mitochondrial fragmentation in *KO* cells compared to *WT* (Scale bar = 20 μm). **(B)** Number of mitochondria per cell and **(C)** individual mitochondrial volume were quantified. Data are from 15 cells examined from three separate experiments (*n=3*). Values are mean ± SEM; ***P*<0.01.

ONLINE FIGURE XI

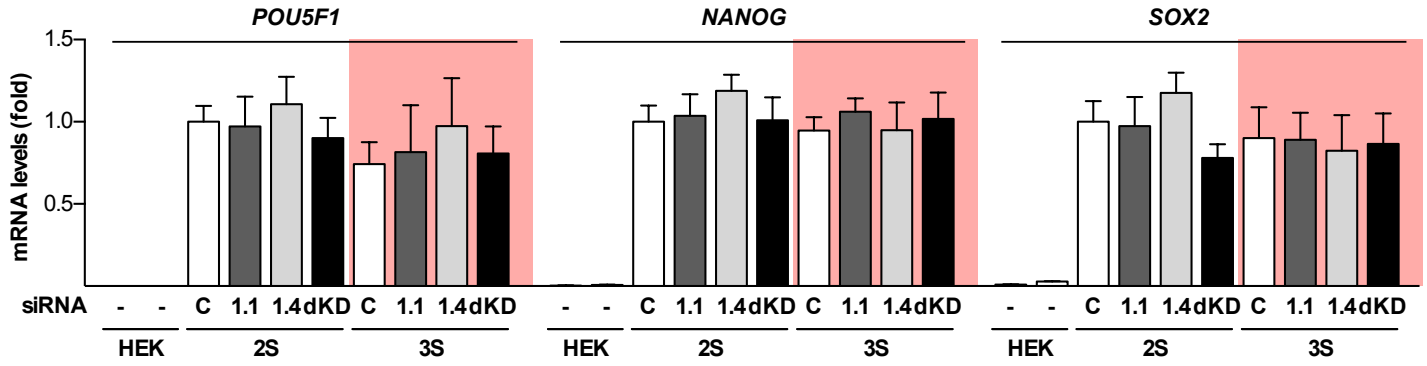

Online Figure XI. siRNA depletion of RCAN1.1 from disomic (2S) and trisomic (3S) iPSC did not affect expression of genes indicative of pluripotency. siRNA-depleted iPSC were analyzed by qPCR for POU class 5 homeobox (POU5F1, also known as OCT3/4), Nanog homeobox (NANOG) and SRY-box 2 (SOX2) expression. HEK293 cells were used as controls for the absence of these markers (*n=4*). Values represent the mean ± SEM.

ONLINE FIGURE XII

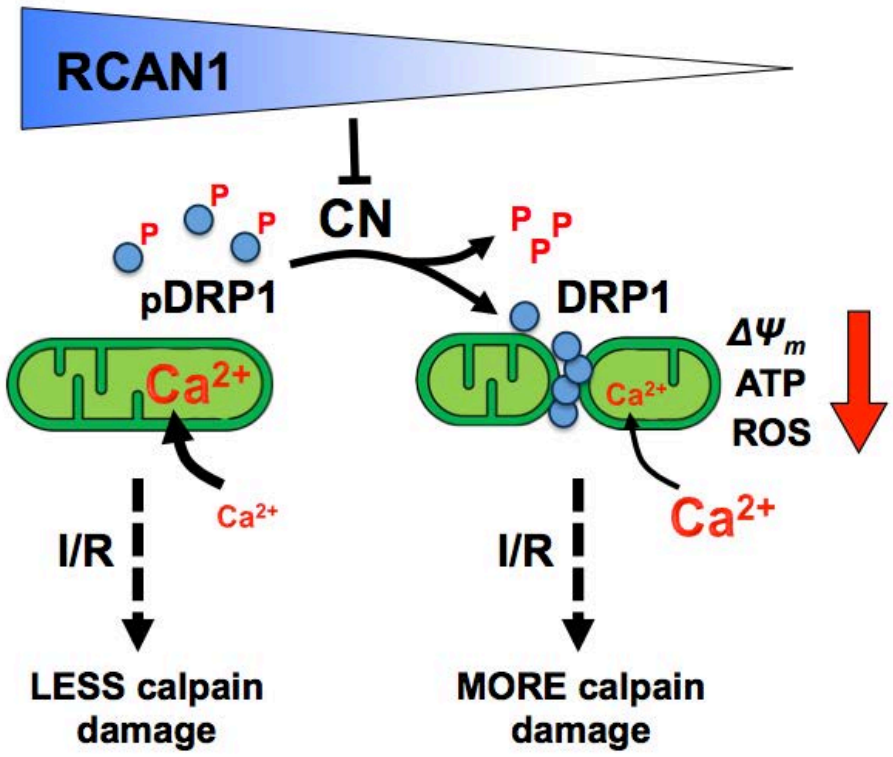

Online Figure XII. Schematic model depicting RCAN1's role in maintaining a metabolically active mitochondrial network. When RCAN1 levels are low, calcineurin (CN) is more easily activated, increasing the potential for translocation of DRP1 to mitochondria to promote fission. The resulting mitochondrial population has a lower membrane potential with decreased O_2 consumption, ROS generation, and capacity for mitochondrial Ca^{2+} uptake. As a consequence cytosolic Ca^{2+} remains elevated longer following I/R increasing CAPN-mediated damage. Increased RCAN1 levels helps preserve fusion and reduce I/R activation of CAPN.

ONLINE FIGURE XIII

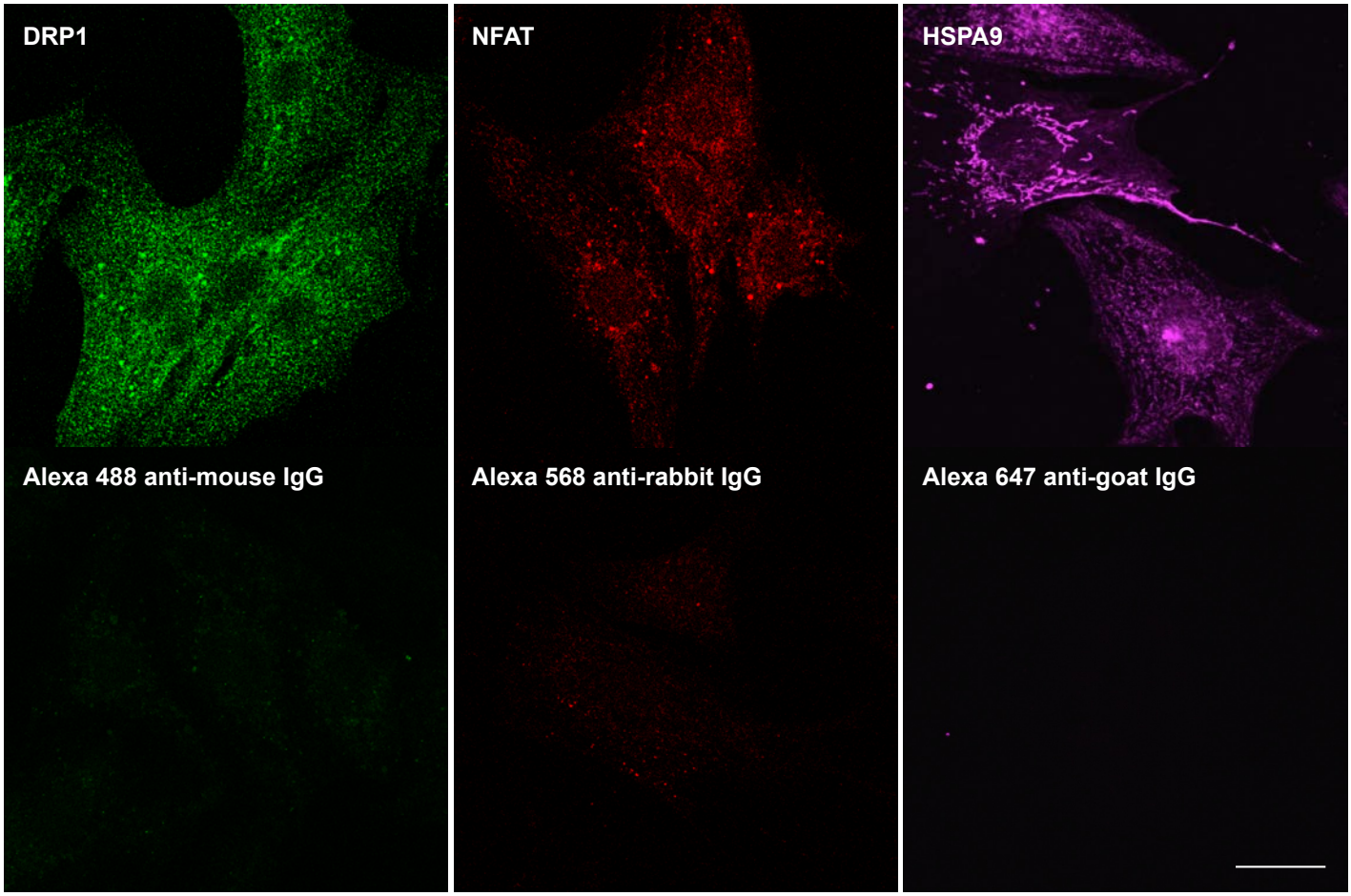

Online Figure XIII. IgG controls for DRP1, NFAT and HSPA9 immunofluorescences. Representative confocal images of immunocytochemistry for DRP1 (green), NFAT (red), mitochondrial HSPA9 (magenta) and their respective controls of IgG-alexa conjugated secondary antibodies in NRVM. Scale bar: 20 μm.